

Proof Transfer for Neural Network Verification

Christian Sprecher

Nostic Solutions AG[†]

christian.sprecher@nostic.ch

Marc Fischer*

ETH Zurich, Switzerland

Dimitar I. Dimitrov

ETH Zurich, Switzerland

dimitar.iliev.dimitrov@inf.ethz.ch

Gagandeep Singh
UIUC[‡] & VMware Research
ggnuds@illinois.edu

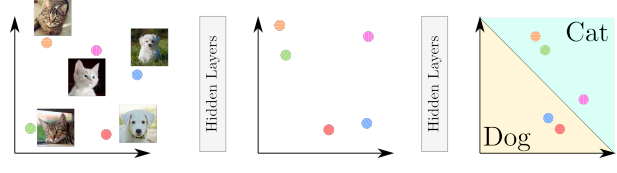
We introduce the novel concept of proof transfer for neural network verification. We show that by generating proof templates that capture and generalize existing proofs, we can speed up subsequent proofs. In particular we create these templates from previous proofs on the same neural network and consider two cases: (i) where the proofs are created online when verifying other properties and (ii) where the templates are created offline using a dataset. We base our methods on three key hypotheses of neural network robustness proofs. Our evaluation shows the potential of proof transfer for benefitting robustness verification of neural networks against adversarial patches, geometric, and ℓ_∞ -perturbations.

1 Introduction

The success of neural networks across a wide range of application domains [24, 42] has triggered substantial interest in understanding their decision making properties. An interesting recent observation in this direction [24, 45] discovered that semantically similar inputs (e.g., two similar cats) produce similar activations (neuron values) at the internal layers of the network. We illustrate this observation in Fig. 1a where similar images are mapped to activation vectors closer to each other at the particular hidden layer than to other inputs. Further, as deeper layers extract more abstract features (e.g., cat’s ears) than earlier layers, the similarity between activations at those layers also increases.

Robustness verification. In parallel to studying neural network decision making, recent years have seen the emergence of an area focused on formally verifying robustness of these models to adversarial perturbations [1, 7–9, 12–14, 17, 21, 22, 28, 32, 38, 40, 41, 43, 44, 46, 47, 50–52, 54]. Conceptually, these methods work by propagating sets of inputs (captured in symbolic form) through the network, producing abstractions of all possible activations at the hidden layers. We illustrate the process in Fig. 1b where we (symbolically) propagate an input region (capturing perturbations to the center point). Robustness verification succeeds if the output abstract shapes provably classify to the same label as the input point which is indeed the case for our example.

Martin Vechev
ETH Zurich, Switzerland
martin.vechev@inf.ethz.ch



(a) Semantically similar inputs have similar neuron activations.

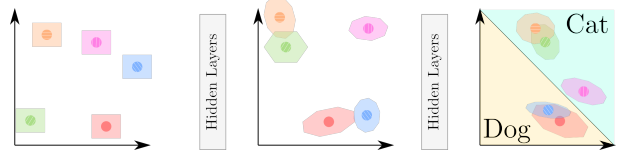


Figure 1. Two hypotheses: similarity on concrete points (due to [24, 45]) and similarity of abstract shapes (our work).

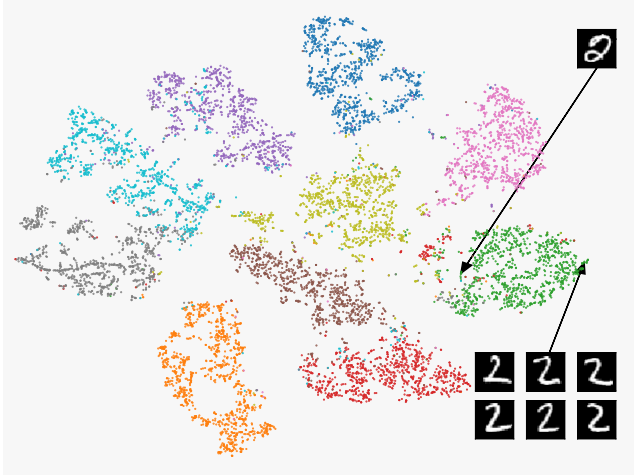
This work: proof similarity and proof transfer. An intriguing hypothesis stemming from the observation that similar inputs trigger similar activations, is that similar input regions should produce similar abstractions at hidden layers. In this work we pose and investigate this hypothesis. We confirm that indeed, the abstract shapes obtained for similar input regions tend to overlap in a large number of dimensions, with the overlap increasing in deeper layers. We illustrate this point in Fig. 1b. Following this hypothesis, we also observe that an abstract shape can sometimes contain another one, and that an approximation which captures a set of abstract shapes may still verify correctly, despite including additional points.

Based on these observations, we then introduce the concept of *proof transfer*, which allows us to leverage abstractions computed for a set of input regions, in order to compute the abstraction for an unseen (similar) input region. We show how to instantiate this concept across several specifications (e.g., ℓ_∞ , geometric, and patch robustness) and scenarios (e.g., reusing proofs from both the test and training datasets), and benefit by reducing the overall verification effort. We note that the idea of proof transfer is orthogonal to existing certification efforts as these consider one input region at a time.

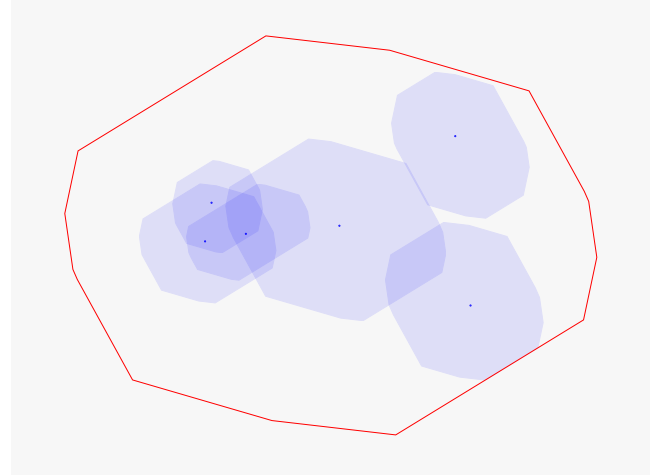
*Main contact

[†]Work performed while at ETH Zurich.

[‡]University of Illinois at Urbana-Champaign



(a) Activations at intermediate layer h of a neural network that classifies the MNIST [26] handwritten digits. Inputs of the same label are colored the same. The 2-dimensional representation is obtained via a TSNE [29] embedding, which aims to preserve the relative ℓ_2 distance between points. Thus semantically similar points are close together.



(b) Dots show activations at layer h for the six similar '2's (left). The blue regions outline the abstract shapes obtained from propagating $\mathcal{I}_\epsilon(\mathbf{x})$ for each of them using the Box abstraction [18, 31]. The red outline shows the box tightly containing all abstract shapes. The two-dimensional representation is obtained via principal component analysis.

Figure 2. (left) low dimensional representation of the activation patterns at an intermediate layer in a handwritten digit classifier. Semantically similar inputs are clustered together. The six images of the digit '2' at the bottom are neighbors (both in projected and high dimensional space). They display similar styles of two, while distant points display other styles. (right) shows the activations for the same 6 images (blue dots) along with the region captured by propagating small perturbations using the Box abstraction. We provide technical details in App. C.

Main Contributions. Our key contributions are:

- A framing of several intriguing observations concerning neural network proofs (§2).
- A framework for transferring proofs leveraging the above properties (§4), illustrating the concept on an example (§3).
- An instantiation of our framework for the task of patch and geometric certification (§5), as well as an instantiation for ℓ_∞ -robustness verification, where we leverage proofs from training data to shortcut proofs on unseen testing inputs (§6).
- A thorough evaluation of the above instantiations, validating our hypotheses on proof similarity and demonstrating the usefulness of proof transfer: we show that significant proof reuse can be obtained (i.e., 94 %) enabling verification speed-ups (§7).

2 Hypotheses for Robustness Proofs

In this section we formulate and discuss several interesting hypotheses about verification proofs of classification robustness. Robustness verification is an instance of local certification: proving a property ψ given a region $\mathcal{I}(\mathbf{x})$ formed around the input \mathbf{x} . The problem is formally stated as follows:

Problem 1 (Local neural network verification). *For an input \mathbf{x} , neural network N , input region $\mathcal{I}(\mathbf{x})$ and postcondition ψ verify that $\forall \mathbf{y} \in \mathcal{I}(\mathbf{x})$. $N(\mathbf{y}) \vdash \psi$.*

To tackle this problem, existing verifiers symbolically propagate $\mathcal{I}(\mathbf{x})$ through the network N , resulting in an abstract shape at each layer, finally checking if the last abstract shape implies ψ . In the case of robustness certification, where one tries to prove classification invariance to adversarial examples [6, 45], a common input region is ℓ_∞ -bounded additive noise, defined as $\mathcal{I}_\epsilon(\mathbf{x}) := \{\mathbf{y} \mid \|\mathbf{x} - \mathbf{y}\|_\infty \leq \epsilon\}$. Here, ϵ defines the size of the maximal perturbation to \mathbf{x} while ψ denotes classification to the same class as \mathbf{x} . In the remainder of this section we illustrate different choices for $\mathcal{I}(\mathbf{x})$, but assume that ψ denotes classification invariance.

Proof similarity. We let $h(\mathbf{x})$ denote the activations at an intermediate layer h in a given neural network for an input \mathbf{x} . As mentioned earlier, it was established by [24] that for semantically similar inputs \mathbf{x} and \mathbf{y} , $h(\mathbf{x})$ and $h(\mathbf{y})$ are close in Euclidean norm. We showcase this hypothesis in Fig. 2a where activations of semantically similar inputs appear visually closer together. Further, as shown in Fig. 1, because deeper layers extract more abstract features, this similarity is expected to increase.

By lifting the hypothesis from concrete points to sets of points (represented by abstract shapes computed by a verifier), we arrive at the following hypothesis. Here, for notational convenience, we let $h(\mathcal{I}(\mathbf{x}))$ denote the abstract region obtained after layer h by propagating $\mathcal{I}(\mathbf{x})$ from the beginning all the way through layer h .

Hypothesis 1. *For semantically similar inputs \mathbf{x}, \mathbf{y} , where $\mathcal{I}(\mathbf{x})$ and $\mathcal{I}(\mathbf{y})$ are certified as robust, $h(\mathcal{I}(\mathbf{x}))$ and $h(\mathcal{I}(\mathbf{y}))$ are numerically similar (their projections in many dimensions overlap). The overlap increases with network depth.*

We performed an extensive quantitative study of this hypothesis for \mathcal{I}_ϵ (discussed in §7.1) and find it indeed holds on different networks, verifiers, and ϵ .

In Fig. 2b, we depict the activations at layer h (blue dots in figure) for the six similar '2's shown in Fig. 2a. The blue region around each dot visualizes the box $[17, 18, 31]$ abstract shape at the given layer (projected onto two dimensions), obtained by propagating $\mathcal{I}_\epsilon(\mathbf{x})$ (with $\epsilon = 0.1$). The figure illustrates that the shapes do overlap in two dimensions, and indeed we confirm significant overlap when we consider all dimensions. We note that abstractions that incur more imprecision than others, naturally show higher overlap. However, we restrict our hypothesis to inputs \mathbf{x} for which $\mathcal{I}(\mathbf{x})$ can be verified robust because in this case, the abstractions cannot become too imprecise as otherwise certification would fail.

Proof sharing. Further investigation of the above hypothesis suggests an interesting underlying property: at an intermediate layer h , abstract shapes obtained from similar inputs can share their proofs for the remaining part of the network. We now consider two instantiations of this high-level observation.

The first instantiation states that we can combine the abstract shapes of similar inputs into an abstract region and proceed to successfully prove robustness with that region jointly for all inputs.

Hypothesis 2. *Given a set of semantically similar inputs \mathbf{x}^i and their corresponding input regions $\mathcal{I}(\mathbf{x}^1), \dots, \mathcal{I}(\mathbf{x}^n)$ that are verified robust, the abstract region which approximates $h(\mathcal{I}(\mathbf{x}^1)), \dots, h(\mathcal{I}(\mathbf{x}^n))$ can also be proved robust when propagated through the remainder of the network.*

This is illustrated in Fig. 2b which shows the projection of the approximation containing all regions in red. This red region may contain more points than the union of points found in the individual regions (due to over-approximation), yet one can still verify it as robust. We provide a quantitative study of this hypothesis in §7.1 and find that 94 % of the groups constructed as in Fig. 2b can be verified robust.

The second instantiation states that one abstract region could subsume another even when the corresponding input regions obtained from the *same* \mathbf{x} do contain eachother.

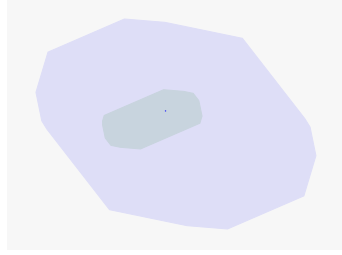


Figure 3. The abstract shape (box abstraction) for input region $\mathcal{I}_\epsilon(\mathbf{x})$ (blue) contains the abstract shape for the input region $\mathcal{I}_p(\mathbf{x})$ (adversarial patch) in green.

Hypothesis 3. *We can often observe input regions $\mathcal{I}_i(\mathbf{x})$ and $\mathcal{I}_j(\mathbf{x})$ where $h(\mathcal{I}_i(\mathbf{x})) \subseteq h(\mathcal{I}_j(\mathbf{x}))$ even though $\mathcal{I}_i(\mathbf{x}) \not\subseteq \mathcal{I}_j(\mathbf{x})$.*

We substantiate the prevalence of this hypothesis in the context of robustness certification of networks against adversarial patches [11]. To visualize the idea, let \mathcal{I}_p denote an input region obtained by placing a random 2×2 patch on the input image \mathbf{x} (arbitrary changes are allowed inside the patch). Fig. 3 shows one of the abstract shapes (for \mathcal{I}_ϵ) taken from Fig. 2b (in blue), along with the abstract shape (in green) obtained for \mathcal{I}_p . Here we observe that $h(\mathcal{I}_p(\mathbf{x})) \subseteq h(\mathcal{I}_\epsilon(\mathbf{x}))$ yet $\mathcal{I}_p(\mathbf{x}) \not\subseteq \mathcal{I}_\epsilon(\mathbf{x})$. Empirically, we find this hypothesis to hold in up to 77 % of cases for randomly placed patches, discussed in §7.1. We also show substantial overlap for geometric perturbations.

3 Overview of Proof Transfer

In this section we present methods which can transfer and leverage proofs for one input region so to prove robustness of other input regions. In turn, this allows us to reduce the proof effort for the entire dataset.

As a running example we consider the simple feed forward neural network N with ReLU activations, shown in Fig. 4, consisting of four layers: an input layer, two hidden layers and an output layer with two neurons each. An affine transform is applied between every two layers, and in addition the affine transform followed by a $\text{ReLU}(\cdot) := \max(\cdot, 0)$ is applied between the hidden layers. Values are propagated left-to-right by multiplying them by the weight on the edge and then summing over all edges entering a node and adding the bias term denoted next to the node. Next, the ReLU (denoted R) function is applied to this sum. In a classification setting, the class with the highest output is considered the predicted class. We let \mathbf{x} , $h_1(\mathbf{x})$, $h_2(\mathbf{x})$ and $N(\mathbf{x})$ denote the input, the activations in the first and second hidden layer and the output of the neural network, respectively.

Here we consider a perturbation \mathcal{I}_ϵ , specifying ℓ_∞ -noise of magnitude $\epsilon = 0.5$, and our goal will be to show that the whole input region $\mathcal{I}_\epsilon(\mathbf{x})$ certifiably classifies to class 0, that is, $N_1(\mathcal{I}_\epsilon(\mathbf{x})) > N_2(\mathcal{I}_\epsilon(\mathbf{x}))$ (meaning any value in the set

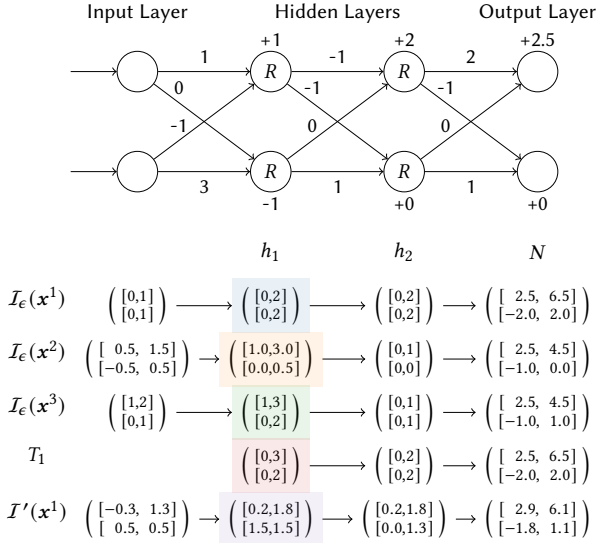


Figure 4. Feed forward network N with hidden layer activations h_1, h_2 . Inputs are propagated left to right along the edges, multiplied with the weight along the edge and summed in the next node, where the bias shown below or above the node is added and the ReLU activation function $R(t) = \text{ReLU}(t) := \max(t, 0)$ is applied.

that the first output neuron can take is strictly greater than any value in the set that the second output neuron can take).

To illustrate the concepts, we use the simple Box abstraction for propagating $I_\epsilon(x)$ where $\begin{pmatrix} [a,b] \\ [c,d] \end{pmatrix}$ denotes a vector where the first component lies between a and b and the second between c and d . For ease of notation, we apply the functions h_1, h_2 and N to points as well as boxes, assuming the standard abstract transformers for box arithmetic.

For inputs $x^1 = \begin{pmatrix} 0.5 \\ 0.5 \end{pmatrix}$ and $x^2 = \begin{pmatrix} 1 \\ 0 \end{pmatrix}$, we show the corresponding propagation of $I_\epsilon(x)$ in Fig. 4. Since all possible values for the second component of the output $N(I_\epsilon(x))$ for x^1 and x^2 ($[-2, 2]$ and $[-1, 0]$, respectively) are less than the lower bound of the first component (2.5 for both inputs) we can verify the classification for both inputs is robust. Similarly, we can show that the same robustness property holds for a new input $x^3 = \begin{pmatrix} 1.5 \\ 0.5 \end{pmatrix}$.

Comparing the proofs for x^1 and x^3 we note that at the second hidden layer we have $h_2(I_\epsilon(x^3)) \subseteq h_2(I_\epsilon(x^1))$ (as $[0, 1] \subseteq [0, 2]$) even though $I_\epsilon(x^3) \not\subseteq I_\epsilon(x^1)$. Thus, if we have already proved correct classification for $I_\epsilon(x^1)$, we can reuse this proof after asserting $h_2(I_\epsilon(x^3)) \subseteq h_2(I_\epsilon(x^1))$, as a result shortcircuiting the verification of x^3 .

Proof Transfer between inputs. However, containment such as the above is rare in practice and often only happens in deeper layers, thus diminishing gains from proof transfer. Thus, to obtain benefits, we need to somehow apply proof transfer earlier in the network. For our example, assume we are trying to verify x^3 and let us consider the first hidden

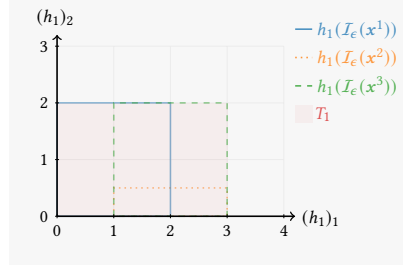


Figure 5. Abstract shapes in the first hidden layer h_1 . The dimensions are shown on the x and y -axis respectively.

layer h_1 . Fig. 4 shows these abstract shapes distinctly colored, while Fig. 5 depicts them geometrically in the corresponding colors. We observe that $h_1(I_\epsilon(x^3))$ is not contained in $h_1(I_\epsilon(x^1))$ or $h_1(I_\epsilon(x^2))$. However, following Hypothesis 2, we can compute the convex hull of the two shapes, that is, $T_1 = h_1(I_\epsilon(x^1)) \sqcup h_1(I_\epsilon(x^2))$ and obtain the template T_1 , shaded in red in Fig. 5. Here, \sqcup denotes the join (the smallest box containing both operands). Propagating T_1 further through the network allows us to successfully verify that the classification is robust even if T_1 is the intermediate output. T_1 region includes $h_1(I_\epsilon(x^3))$ and can thus be used to shortcut its verification at the first hidden layer. This showcases how we can create templates for previously unseen data points. Like this, in §6, we compute templates offline on the training set, allowing for faster verification of new inputs.

To illustrate the speed-up expected from proof transfer, consider a feed forward neural network with L layers and n neurons each. Verification using Box abstractions then has a time complexity of $O(Ln^2)$. If we create a template at layer $k < L$, and the template contains the input region propagated to layer k , then the complexity is reduced to $O(kn^2)$ plus a linear term for checking template containment. Crucial to obtaining end-to-end speed-ups is that the cost of the containment check does not exceed the gains from stopping the propagation at layer k . In case the template is not sufficient to prove the given input region, the full verification must be computed by further propagating from layer k to the end. Suppose that the constructed template contains the proof for a given input with a probability ρ , then the overall complexity of our verification procedure is $O((\rho k + (1 - \rho)L)n^2)$ in expectation. It can be observed that the gains in obtained speedup increase with ρ .

Proof Transfer between different perturbations. So far, we considered different inputs x^1, x^2 and x^3 with the same perturbation I_ϵ . We now discuss an example of proof transfer on the same input x^1 but for different perturbations I_ϵ and I' , as motivated by Hypothesis 3. Consider the input region $I'(x) := \{y \mid |x_1 - y_1| \leq 0.8\}$, where subscript 1 denotes the first dimension. For input x^1 , this results in the region $I'(x^1) := \begin{pmatrix} [-0.3, 1.3] \\ [0.5, 0.5] \end{pmatrix}$ as shown in Fig. 4. We now have that $h_1(I'(x^1)) \subseteq h_1(I_\epsilon(x^1))$ even though $I'(x^1) \not\subseteq I_\epsilon(x^1)$.

This allows us to use $h_1(\mathcal{I}_\epsilon(\mathbf{x}^1))$ as a proof template for \mathcal{I}' . We will apply this kind of proof transfer in §5 to allow for fast verification of multiple different perturbations on a given input \mathbf{x} . Here, template generation is performed online and amortized by the fast verification of other regions.

Related Work: Proof sharing over similar Network. Before formally introducing our framework, briefly discuss conceptually related work, where verification results are shared between similar neural networks. Ashok et al. [2] simplify neural networks before applying verification algorithms to the simplified neural network. The proof obtained on the simplified neural network can then be transferred back to the original neural network. Paulsen et al. [35, 36] analyses the difference between two closest related neural networks, exploring their structural similarity in the analysis. Cheng and Yan [10] reuse previous analysis results after a neural network is slightly modified, e.g. fine-tuned. In contrast, we consider the neural network to be fixed and apply proof transfer over similar, but distinct, input regions.

4 Proof Transfer with Templates

We now introduce our formal framework of proof transfer. We decompose the notion of proof transfer into two sub-problems: the generation of proof templates and the matching of abstract shapes to these templates.

In the following we consider a network $N : \mathbb{R}^m \rightarrow \mathbb{R}^n$ composed of L layers. For $k < L$, we let $N_{1:k}$ denote the first k layers and $N_{k+1:L}$ denote the last $L - k$ layers. Further, we consider a verifier V that solves Problem 1 (shown earlier), by taking as input a region $\mathcal{I}(\mathbf{x})$, propagating it through N , and checking ψ on the output abstract shape. We let $V(\mathcal{I}(\mathbf{x}), N_{1:k})$ denote the abstract shape produced by the verifier V at layer k when invoked on input region $\mathcal{I}(\mathbf{x})$. Further, $V(T, N_{k+1:L})$ denotes the output abstract shape of the verifier when it is given the region T at layer k (hence, the next layer to push T through is $k + 1$).

Our goal in proof transfer is to construct a suitable template T at layer k by using abstract shapes produced by the verifier at k (as illustrated in §3), so that T captures abstract shapes at layer k obtained from propagating unseen $\mathcal{I}(\mathbf{x})$, yet still ensure that T verifies. As it can be challenging to capture all input regions with a single T , we allow a set of templates \mathcal{T} . The problem of finding a set of templates is formally stated as: Problem 2.

Problem 2 (Template Generation). *For a given neural network N , layer k , verifiers V_Q, V_T and postcondition ψ , find a set of templates \mathcal{T} with $|\mathcal{T}| \leq m$ such that:*

$$\begin{aligned} \max_{(\mathbf{x}, \mathcal{I}) \sim \mathcal{P}} & \mathbb{E} \left[\bigvee_{T \in \mathcal{T}} V_Q(\mathcal{I}(\mathbf{x}), N_{1:k}) \subseteq T \right] \\ \text{s.t. } & V_T(T, N_{k+1:L}) \vdash \psi \text{ for } T \in \mathcal{T} \end{aligned} \quad (1)$$

Here \mathcal{P} denotes the distribution of expected input regions defined by \mathbf{x} and \mathcal{I} . This formulation allows for various scenarios including \mathbf{x} and \mathcal{I} to be jointly distributed, but also for a fixed \mathcal{I} and a \mathbf{x} drawn from a data distribution \mathcal{D} , as well as a fixed \mathbf{x} and a \mathcal{I} drawn from a set of possible specifications. Further, note that the verifier V_Q , which propagates new input regions to layer k and the verifier V_T , used to verify templates, may employ different verification strategies (e.g., exact vs inexact methods or different abstractions).

Problem 2 does not necessarily require that the templates T are created from previous proofs. However, recalling the hypotheses discussed in §2, in §5 and §6 we will infer the templates from previously obtained robustness proofs.

To leverage proof transfer once the templates \mathcal{T} are obtained, we need to be able to match an abstract region $S = V_Q(\mathcal{I}(\mathbf{x}), N_{1:k})$ to a template in \mathcal{T} :

Problem 3 (Template Matching). *Given a set of templates \mathcal{T} at layer k of a neural network N , verifier V_Q , a new input region $\mathcal{I}(\mathbf{x})$, determine whether there exists a $T \in \mathcal{T}$ such that $S \subseteq T$, where $S = V_Q(\mathcal{I}(\mathbf{x}), N_{1:k})$.*

Together, Problems 2 and 3 outline a general framework for proof transfer, permitting many instantiations such as the settings previously discussed in §3. In the next section we discuss template generation assuming templates are represented by some abstract domain D . After that, we will see how to instantiate D so that template generation and matching can be efficient. We note here that Problems 2 and 3 present an inherent trade-off: Problem 3 can be solved most efficiently for small values of $m = |\mathcal{T}|$ and simpler representations of T (allowing faster checking of $S \subseteq T$). Alternatively, Eq. (1) can be maximized by large m and T represented by complex shapes, thus attaining high precision.

5 Online Template Generation

We now consider an instantiation of Problem 2, where we are given an input \mathbf{x} and properties $\mathcal{I}_1, \dots, \mathcal{I}_r$ to verify. To instantiate proof transfer, we first create the set of templates \mathcal{T} and subsequently verify $\mathcal{I}_1, \dots, \mathcal{I}_r$ using \mathcal{T} . Depending on the magnitude of r , template generation must be relatively fast in order to obtain a verification speedup.

To formalize this setting, we instantiate Problem 2, for a distribution \mathcal{P} , over a single fixed \mathbf{x} and multiple perturbations $\mathcal{I}_1, \dots, \mathcal{I}_r$.

We discuss our template generation algorithm for this online setting in §5.1, and then instantiate it for the verification of robustness to adversarial patches and geometric perturbations in §5.2 and §5.3, respectively.

5.1 Template Generation

Following the insight that abstract shapes for some perturbations include those of others (Hypothesis 3), we slightly relax the problem in order to create the templates T_i from abstract shapes $V_T(\hat{\mathcal{I}}_i(\mathbf{x}), N_{1:k})$ for some $\hat{\mathcal{I}}_i$. Further, we let \mathcal{P}_T denote

the categorical distribution over $\mathcal{I}_1, \dots, \mathcal{I}_r$. We note that the $\hat{\mathcal{I}}_i$ are not directly related to $\mathcal{I}_1, \dots, \mathcal{I}_r$. Then, for a particular layer k , image \mathbf{x} and number of templates m we optimize

$$\arg \max_{\hat{\mathcal{I}}_1, \dots, \hat{\mathcal{I}}_m} \mathbb{E}_{\mathcal{I} \sim \mathcal{P}_{\mathcal{I}}} \left[\bigvee_{i=1}^m V_Q(\mathcal{I}(\mathbf{x}), N_{1:k}) \subseteq T_i \right] \quad (2)$$

where $T_i = \alpha_D(V_T(\hat{\mathcal{I}}_i(\mathbf{x}), N_{1:k}))$
s.t. $V(T_i, N_{k+1:L}) \vdash \psi$ for $i \in 1, \dots, m$.

Here α_D denotes the conversion from an abstract region Z into an element in the domain D (e.g., assuming the domain employed by V_T is more precise than D , α_D denotes its further abstraction). This problem is solved by selecting $\hat{\mathcal{I}}_1, \dots, \hat{\mathcal{I}}_m$ such that the resulting templates cover as much as possible of the abstract regions obtained from propagating $\mathcal{I} \sim \mathcal{P}_{\mathcal{I}}$. To this end, in §5.2 and §5.3 we will choose parametric $\hat{\mathcal{I}}_i$ and solve Eq. (2) by optimizing over these parameters.

5.2 Robustness to Adversarial Patches

We now instantiate the above scheme in order to verify robustness against adversarial patches in image classification [11]. Consider an attacker that is allowed to arbitrarily change any $p \times p$ patch of the image. For such a patch over pixel positions $([i, i+p-1] \times [j, j+p-1])$, the corresponding perturbation is

$$\mathcal{I}_{p \times p}^{i,j}(\mathbf{x}) := \{\mathbf{y} \in [0, 1]^{h \times w} \mid \forall (k, l) \in \pi_{p \times p}^{i,j}. \mathbf{y}_{k,l} = \mathbf{x}_{k,l}\}$$

where $\pi_{p \times p}^{i,j} = \{(k, l) \mid \begin{array}{l} k \in 1, \dots, h \\ l \in 1, \dots, w \end{array}\} \setminus \{(k, l) \mid \begin{array}{l} k \in i, \dots, i+p-1 \\ l \in j, \dots, j+p-1 \end{array}\}$

where h and w denote the height and width of \mathbf{x} . To prove robustness for an arbitrarily placed $p \times p$ patch, however, one must consider the perturbation set $\mathcal{I}_{p \times p}$

$$\mathcal{I}_{p \times p}(\mathbf{x}) := \bigcup_{\substack{i \in \{1, \dots, h-p+1\} \\ j \in \{1, \dots, w-p+1\}}} \mathcal{I}_{p \times p}^{i,j}$$

To prove robustness based on $\mathcal{I}_{p \times p}$, Chiang et al. [11] separately verify $\mathcal{I}_{p \times p}^{i,j}(\mathbf{x})$ for all $i \in \{1, \dots, h-p+1\}, j \in \{1, \dots, w-p+1\}$. For example, with $p=2$ and an 28×28 MNIST image, this approach requires 729 individual proofs. Because the different proofs for $\mathcal{I}_{p \times p}$ share similarities, one can apply proof transfer. We solve Eq. (2) for m templates with an input perturbation $\hat{\mathcal{I}}_i$ per template.

We empirically found ℓ_∞ -templates to capture these patch perturbations well (§7.1). In fact, we find ℓ_∞ to be a surprisingly universal input region, as abstract shapes obtained from it form templates for many other input regions (we will also showcase its applicability for geometric perturbations). Thus, we consider m template perturbations of the form

$$\hat{\mathcal{I}}_i(\mathbf{x}) := \{\mathbf{y} \mid \|\mathbf{x}_{\pi_i} - \mathbf{y}_{\pi_i}\|_\infty \leq \epsilon_i\},$$

where π_i denotes a subset of pixels of the input image. In particular, we consider π_1, \dots, π_m , such that they partition the set of pixels in the image.

Thus, we recast the template generation in Eq. (2) as:

$$\arg \max_{\substack{\pi_1, \dots, \pi_m \\ \epsilon_1, \dots, \epsilon_m}} \mathbb{E}_{\mathcal{I} \sim \mathcal{P}_{\mathcal{I}}} \left[\bigvee_{i=1}^m V_Q(\mathcal{I}(\mathbf{x}), N_{1:k}) \subseteq T_i \right] \quad (3)$$

where $T_i = V_T(\hat{\mathcal{I}}_i(\mathbf{x}), N_{1:k})$
s.t. $V_T(T_i, N_{k+1:L}) \vdash \psi$ for $i \in 1, \dots, m$.

In contrast to the setting in §6, where template generation is performed offline, in this section we consider a different trade-off. This is because both template generation, Problem 2, and template matching, Problem 3, are performed online. Thus, we consider small m , and fixed patterns π_1, \dots, π_m . For each $\hat{\mathcal{I}}_i$ we then find the largest ϵ_i (in order to maximize the number of matches), which can still be verified. Note that for $m=1$ this is equivalent to the ℓ_∞ input perturbation \mathcal{I}_ϵ with the maximal verifiable ϵ for the given image. Concretely, we perform binary search over ϵ_i in order to maximize it while still satisfying $V_T(\alpha_D(V_T(\mathcal{I}_i(\mathbf{x}), N_{1:k})), N_{k+1:L}) \vdash \psi$.

We instantiate both V_Q and V_T with a verifier that propagates zonotopes [43].

We represent the obtained templates in the Box domain. While zonotopes seem a natural choice for the template, as they are produced by V_Q , template matching, Problem 3, can not be efficiently evaluated as the containment check $S \subseteq T$ is computationally hard. However, for a zonotope S and box T , the $S \subseteq T$ can be computed efficiently. We let $\mathbf{l}^T, \mathbf{u}^T \in \mathbb{R}^d$ denote vectors containing the lower and upper bound of box T in each dimension. A zonotope S is of the form

$$S = \{z \in \mathbb{R}^d \mid z = \mathbf{a} + \mathbf{A}\mathbf{e}, \mathbf{e} \in [-1, 1]^p\}, \quad (4)$$

parametrized with $\mathbf{a} \in \mathbb{R}^d$ and $\mathbf{A} \in \mathbb{R}^{d \times p}$. To check $S \subseteq T$, we first compute the bounding box of S given by $\mathbf{l}^S, \mathbf{u}^S \in \mathbb{R}^d$ with $\mathbf{l}_i^S = \mathbf{a}_i - \sum_{j=1}^p |A_{i,j}|$ and $\mathbf{u}_i^S = \mathbf{a}_i + \sum_{j=1}^p |A_{i,j}|$. Then we can assert $\mathbf{l}_i^T \leq \mathbf{l}_i^S \wedge \mathbf{u}_i^S \leq \mathbf{u}_i^T$ to show $S \subseteq T$. A Box T can directly be encoded as a Zonotope, thus allowing V_T to be invoked on a template T .

Templates at multiple layers. By slightly extending the previous approach, it is possible to create templates at multiple layers at once. Formally, we instantiate Eq. (3) for multiple values of k at once. With templates at layers k and k' (with $k \leq k'$) we first try to match the propagated shape against templates at layer k and if this fails, we propagate it further to layer k' and again try to match the proof.

To this end, in practice we use binary search to first find the maximal ϵ_i for which $V_T(\mathcal{I}_i(\mathbf{x}), N) \vdash \psi$. Then, for each considered layer k , we apply α_D to the abstract shape to obtain $T_i^k := \alpha_D(V_T(\mathcal{I}_i(\mathbf{x}), N_{1:k}))$. As the resulting T_i^k may not necessarily be verified, due to the additional volume introduced by representing the zonotope as a box, we perform a second binary search on a scaling factor to uniformly decrease dimensions of T_i^k such that $V_T(T_i^k, N_{k+1:L}) \vdash \psi$. We repeat this process for other layers as well.

5.3 Geometric Robustness

Geometric robustness verification [4, 16, 27, 33, 37, 44] aims to verify robustness to geometric transformations such as image rotations or image translations. These transformations typically include an interpolation operation. We demonstrate this on the example of a rotation R_γ by $\gamma \in \Gamma$ degrees for an interval Γ (e.g., $\gamma \in [-5, 5]$), for which we consider the perturbation $\mathcal{I}_\Gamma(\mathbf{x}) := \{\mathbf{y} \mid \mathbf{y} = R_\gamma(\mathbf{x}), \gamma \in \Gamma\}$. We note that unlike ℓ_∞ and patch verification, the input regions for geometric transformations are non-linear and have no closed-form solutions. Thus, an overapproximation of the input region is obtained [4]. For large Γ , the approximate input region $\mathcal{I}_\Gamma(\mathbf{x})$, can be too coarse resulting in imprecise verification. Hence, in order to assert ψ on \mathcal{I}_Γ , existing state-of-the-art approaches, e.g., Balunovic et al. [4], split Γ into b smaller ranges $\Gamma_1, \dots, \Gamma_b$ and then verify $(\mathcal{I}_{\Gamma_i}, \psi)$ for $i \in 1, \dots, b$.

These smaller perturbations share similarities facilitating proof transfer. We instantiate our approach similar to §5.2. A key difference to §5.2 is that while there are $\mathbf{x} \in \mathcal{I}_{p \times p}^{i,j}(\mathbf{x})$ for all i, j , here in general $\mathbf{x} \notin \mathcal{I}_{\Gamma_i}(\mathbf{x})$ for most i . Therefore, the individual perturbations $\mathcal{I}_i(\mathbf{x})$ do not overlap.

To account for this, we consider m templates and split Γ into m equally sized chunks (unrelated to the b splits) obtaining the angles $\gamma_1, \dots, \gamma_m$ at the center of each chunk. For m templates we then consider the perturbations $\hat{\mathcal{I}}_i := \mathcal{I}_{\epsilon_i}(R_{\gamma_i}(\mathbf{x}))$, where \mathcal{I}_{ϵ_i} denotes perturbation with ℓ_∞ -bounded additive noise with magnitude up to ϵ_i . As in §5.2 we search over ϵ_i to obtain templates at multiple layers.

6 Template Generation on Training Data

After discussing template generation in an online manner we now consider the more challenging offline setting. Here, consider an instantiation of Problem 2, in the setting where $\mathbf{x} \sim \mathcal{D}$ is drawn from the data distribution. As standard in machine learning, we assume that we have access to a large sample from \mathcal{D} , the training set T_{train} . We create \mathcal{T} offline from the training set, and then verify new inputs \mathbf{x} by utilizing \mathcal{T} . What makes this setting challenging is that we require the templates \mathcal{T} to be general enough to generalize to unseen inputs.

We first outline the template generation process in general in §6.1 and then show an instantiation for ℓ_∞ -robustness verification in §6.2 and §6.3.

6.1 Template Generation

We first consider a single \mathcal{I} and then present an extension to multiple $\mathcal{I}_1, \dots, \mathcal{I}_r$. Assuming a sufficiently large T_{train} , where we obtain verification rate $\mathbb{E}_{\mathbf{x} \in T_{\text{train}}} [V_Q(\mathcal{I}(\mathbf{x}), N)]$, we can theoretically construct \mathcal{T} containing all abstract shapes observed at layer k by propagating all $\mathcal{I}(\mathbf{x})$ and taking their possible convex unions. We would then, due to Hypothesis 2, expect to obtain similar verification rates when using \mathcal{T} to certify new input regions. However, in practice this rate will

be diminished by the size of T_{train} , the limit $|\mathcal{T}| \leq m$ on the number of allowed templates (which we add to allow for efficient template matching, Problem 3) and by how well Hypothesis 2 holds in practice on the considered network and input regions.

Thus, in order to optimize Eq. (1) under our constraints, we attempt to find the set of templates \mathcal{T} that contains the most abstract regions at layer k obtained from T_{train} . While this is generally computationally hard, we approximate this with a clustering-based approach. To this end, we first compute the abstract shapes $V_Q(\mathcal{I}(\mathbf{x}), N_{1:k})$ for $\mathbf{x} \in T_{\text{train}}$ and then cluster and merge them. Subsequently, we further merge the obtained templates until we obtain a set \mathcal{T} of m templates. We formalize the template generation procedure in Algorithm 1 and showcase it in Fig. 6.

We first (line 1, Fig. 6a) compute the set \mathcal{V} of abstract shapes at layer k , that can be verified by V_Q . Then, we cluster the abstract regions in \mathcal{V} into n groups \mathcal{G}_i of similar abstract shapes using the function `cluster_shapes` (which we will instantiate in §6.2), showcased by different colors in Fig. 6b. For each group \mathcal{G}_i , we compute its convex hull T in domain D via the join \sqcup_D . If V_T can verify this T , then we add the tuple (T, \mathcal{G}_i) , the template along with all abstract shapes it covers, to the set \mathcal{H} , shown in Fig. 6c. As depicted in Fig. 6d, we attempt to merge pairs of these templates (line 12). To this end, we traverse them in order of their distance d . Here, we use the Euclidean distance between the centers of T_1 and T_2 for $d(T_1, T_2)$. In order to merge (T_1, \mathcal{G}_1) and (T_2, \mathcal{G}_2) , we first compute the set of their contained shapes $\mathcal{G}' = \mathcal{G}_1 \cup \mathcal{G}_2$ (line 13) and then again compute the convex hull $T' = \sqcup_D(\mathcal{G}')$ (line 14). If T' can be verified, we replace (T_1, \mathcal{G}_1) and (T_2, \mathcal{G}_2) by (T', \mathcal{G}') in \mathcal{H} (lines 15 to 21). This procedure is repeated until no templates can be merged. Finally, \mathcal{T} is obtained as the set of the m templates with the most associated abstract shapes (e.g., the largest $|\mathcal{G}|$) in \mathcal{H} .

A potentially more optimal set \mathcal{T} (in terms of abstract shapes contained) could be found by adding $\mathcal{H} \leftarrow \mathcal{H} \cup \{(\alpha_D(P), \{P\}) \mid V_T(\alpha_D(P), N_{k+1:L}) \vdash \psi, P \in \mathcal{G}_i\}$ if verification of T generated from \mathcal{G}_i in line 6 fails. Here $\alpha_D(p)$ convert the abstract shape p to element in the template domain D (e.g., further abstraction). This way, the iterative template merge between lines 10 and 21 could compute a more optimal solution. However, as this is generally computationally infeasible, we refrain from doing so.

Extension to multiple $\mathcal{I}_1, \dots, \mathcal{I}_r$. So far in this section we assumed a single \mathcal{I} . However, the same algorithm can be applied to multiple $\mathcal{I}_1, \dots, \mathcal{I}_r$. Depending on the similarity of the perturbations, a set of templates $\mathcal{T}_1, \dots, \mathcal{T}_r$ can be obtained for each perturbation by applying Algorithm 1 separately or a joint \mathcal{T} by either merging them afterwards or by instantiating \mathcal{V} in line 1 with $\mathcal{V} \leftarrow \{V(\mathcal{I}_i(\mathbf{x}), N_{1:k}) \mid \mathbf{x} \in T_{\text{train}}, V_Q(\mathcal{I}_i(\mathbf{x}), N) \vdash \psi, i \in \{1, \dots, r\}\}$.

Algorithm 1: Template generation over T_{train}

```

Input: training set  $T_{\text{train}}$ , verifiers  $V_Q, V_T$ 
Result: Set  $\mathcal{T}$  of templates,  $|\mathcal{T}| \leq m$ 
1  $\mathcal{V} \leftarrow \{V(\mathcal{I}(\mathbf{x}), N_{1:k}) \mid \mathbf{x} \in T_{\text{train}}, V_Q(\mathcal{I}(\mathbf{x}), N) \vdash \psi\}$ 
2  $\mathcal{G}_1, \dots, \mathcal{G}_n \leftarrow \text{cluster\_shapes}(\mathcal{V})$ 
3  $\mathcal{H} \leftarrow \emptyset$ 
4 for  $i \leftarrow 1$  to  $n$  do
5    $T \leftarrow \sqcup_D(\mathcal{G}_i)$ 
6   if  $V_T(T, N_{k+1:L}) \vdash \psi$  then
7     |  $\mathcal{H} \leftarrow \mathcal{H} \cup \{(T, \mathcal{G}_i)\}$ 
8   end
9 end
10 pairs  $\leftarrow$  all pairs  $(T_1, \mathcal{G}_1), (T_2, \mathcal{G}_2)$  in  $\mathcal{H}$ 
11  $Q \leftarrow$  priority queue over pairs, ordered by  $d(T_1, T_2)$ 
12 foreach pair  $(T_1, \mathcal{G}_1), (T_2, \mathcal{G}_2)$  in  $Q$  do
13    $\mathcal{G}' = \mathcal{G}_1 \cup \mathcal{G}_2$ 
14    $T' = \sqcup_D(\mathcal{G}')$ 
15   if  $V(T', N_{k+1:L}) \vdash \psi$  then
16     |  $\mathcal{H} \leftarrow \mathcal{H} \setminus \{(T_1, \mathcal{G}_1), (T_2, \mathcal{G}_2)\}$ 
17     | remove elements containing  $(T_1, \mathcal{G}_1)$  from  $Q$ 
18     | remove elements containing  $(T_2, \mathcal{G}_2)$  from  $Q$ 
19     | add all pairs  $(T, \mathcal{G}), (T', \mathcal{G}')$  for  $(T, \mathcal{G}) \in \mathcal{H}$ 
      | to  $Q$ 
20   |  $\mathcal{H} \leftarrow \mathcal{H} \cup \{(T', \mathcal{G}')\}$ 
21   end
22 end
23  $\mathcal{T} \leftarrow T$  for  $(T, \mathcal{G}) \in \mathcal{H}$  for the  $m$  largest  $|\mathcal{G}|$ 
24 return  $\mathcal{T}$ 

```

After finding templates in this manner we then perform an additional step called *template extension*, discussed in App. B, in which we linearly enlarge the obtained template.

6.2 Dataset templates for ℓ_∞ robustness

We now instantiate the template generation algorithm for ℓ_∞ -robustness verification \mathcal{I}_ϵ . As in §5.2 and §5.3, we instantiate V_Q with a verifier that propagates zonotopes and V_T with one that performs exact verification via Mixed-Integer Linear Programming (MILP) [46]. The box-encoded templates can be directly verified by the exact verifier V_T . We note that since V_T is strictly more precise than V_Q , the use of templates can potentially allow for *higher* certification rates than directly employing V_Q . While we did not observe this experimentally, it presents an interesting target for further investigation.

We now briefly discuss the properties of the exact verifier V_T , as we require these in the following discussion. Internally, V_T , utilizing the framework from Tjeng et al. [46], proves classification to the correct label l by maximizing the error $e = \max_{i \neq l} \mathbf{n}_i - \mathbf{n}_t$ (asserting that $e < 0$), where \mathbf{n} denotes the output of the neural network (e.g. its logits) over the considered input region. If no counterexample to that assertion can

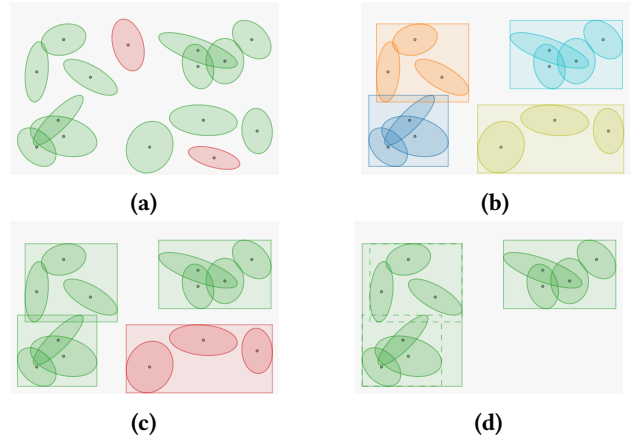


Figure 6. Visualization of Algorithm 1. First, in (a) the abstract shapes at layer k for input regions in the training set are obtained, and restricted to the verifiable ones (green). These are then clustered and their convex hulls in domain D are obtained. (b) shows different clusters in different colors. The convex hulls are then verified (c), and restricted to the verifiable ones (green). Finally in (d), these regions are further merged, if possible, to obtain the set of templates.

be found, it certifies the specification, else it returns a set of counterexamples $\{z_{V,i}\}$ (concrete points in the input region), utilized later, for which this error is maximal. In both cases we can access value e of the error function.

Next, we instantiate `cluster_shapes` with k -means clustering for which we provide a similarity matrix computed as follows: for each pair of abstract shapes $P_1, P_2 \in \mathcal{V}$ we compute $B = P_1 \sqcup_B P_2$, where \sqcup_B denotes their Box join, and use $\exp(e)$ as their distance, where e is obtained from V_T when attempting to verify ψ for B . To obtain a similarity matrix from these distances, we apply a constant shift embedding [39]. As running V_T for each pair (P_1, P_2) is expensive, we only consider the t closest neighbors (in ℓ_2 distance between centers) and set all others to a maximal distance.

6.3 Half-space constraints

To allow for larger templates T , e.g., those that allow to optimize Eq. (1) further by containing more abstract shapes, we extend the template domain D from boxes to boxes with additional half-space constraints. The resulting convex polyhedra, formally called stars [3, 48], allow for larger boxes while the half-space constraints cut-off potentially non-verifiable regions, yet, still allow efficient containment checks $S \subseteq T$.

Formally a star T^S over a box T is denoted as:

$$T^S(C, c) := \{z \in \mathbb{R}^d \mid z \in T \wedge Cz \leq c\} \quad (5)$$

with $C \in \mathbb{R}^{c \times d}, c \in \mathbb{R}^c$.

Here each half-space constraint is described by a hyperplane parameterized by $C_i.$ and $c_i.$

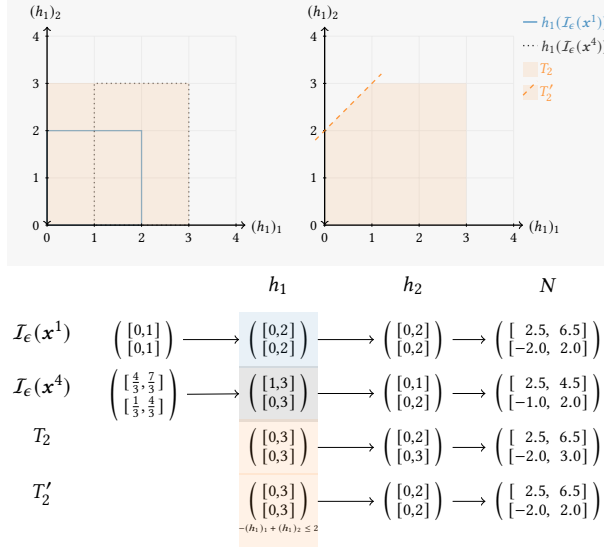


Figure 7. Continuation of the example (§3): T_2 is not verifiable, yet T_2' with additional half-space constraint, is.

The containment check $S \subseteq T^S$ for an abstract shape S , e.g. a zonotope, and star T^S consists of: (i) a containment for the underlying box $S \subseteq T$, and (ii) checking if for each constraint $C_i \cdot z \leq c_i$, maximizing the linear expression $C_i \cdot z$ with respect to S yields an objective $\leq c_i$. For a zonotope S as given in Eq. (4), we have shown the computation of step (i) in §6.2 and can efficiently check step (ii) via $C\mathbf{a} + \sum_{j=1}^p |CA|_j \leq c$.

A star encoded as in Eq. (5) can be directly verified using V_T by adding the half-space constraints as further LP constraints. We now showcase the utility of these hyperplane constraints before describing their generation.

Example (cont.) We illustrate this in Fig. 7, as a continuation of our overview example.

The region T_2 , shaded orange, is obtained by Box join $T_2 = h_1(\mathcal{I}_\epsilon(x^1)) \sqcup h_1(\mathcal{I}_\epsilon(x^4))$. While $h_1(\mathcal{I}_\epsilon(x^1))$ and $h_1(\mathcal{I}_\epsilon(x^4))$ are both verifiable, T_2 is not. However, if we add a new half-space constraint given by $C := (1, -1)$ and $c := (2)$, the resulting template T_2' (a star) becomes verifiable.

Obtaining half-space constraints. In the template generation process we utilize boxes as before. However, whenever we fail to verify a template with V_T (e.g., lines 6 and 15 in Algorithm 1), we attempt to add a half-space constraint. We repeat this up to n_{hs} times resulting in as many constraints. We leverage the exact verifier V_T for obtaining half-space constraints. Recall V_T either verifies a region or provides a set of counterexamples $\{z_{V,i}\}$. Since we only add additional half-space constraints, if the verification fails we utilize these counterexamples. In the following we assume a single z_V , which in practice is usually the case, and derive a hyperplane that separates z_V from the abstract shape we are trying to verify. If there are multiple $z_{V,i}$, we iterate over them and perform the described procedure for each $z_{V,i}$, that is not already

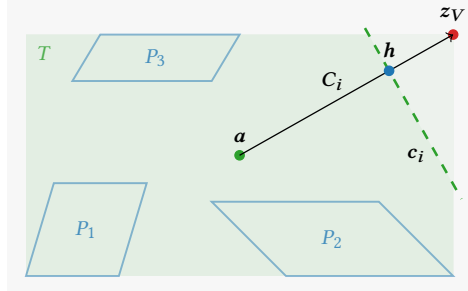


Figure 8. The algorithm used to find half-space constraints, by cutting counterexample z_V from the template T with a hyperplane (C_i, c_i) . The normal of the hyperplane (specified by C_i) is given by the vector between a (the center of T) and z_V . The threshold c_i is chosen such that the hyperplane removes z_V but does not intersect any abstract regions P_1, P_2, P_3 the template T was created from.

cut by the hyperplane found for a previous counterexample. These hyperplanes directly yield the new constraints.

We showcase this in Fig. 8, where the green shaded area T shows the Box join over three abstract regions $T = \bigsqcup_D(\{P_1, P_2, P_3\})$. The individual P_i , shown in blue, are zonotopes, that can be verified individually.

The verification of the green area fails, with the counterexample z_V (red dot) shown in the top right corner. To find a hyperplane that separates z_V from the rest of T , we consider the line from the center a (green dot) of T to the point z_V and a hyperplane orthogonal to it (shown as the dashed line). Thus, adding a row i to the matrix C of the star: $C_i = (z_V - c)^T$. To find offset $h = \lambda a + (1 - \lambda)z_V$ (for $\lambda \in [0, 1]$) along this line to, we consider the value attained for $C_i x$ for x in the verified area (P_1, P_2, P_3) :

$$c_p := \max_{\substack{x \in P \\ P \in \{P_1, P_2, P_3\}}} C_i x.$$

Then, the constant c_i of the new hyperplane is given by $c_i = \kappa c_p + (1 - \kappa)z_V$ for a hyper-parameter κ and $c_z := C_i z_V$.

A high κ puts the hyperplane close to z_V , removes only little volume from the template, while low κ puts it closer to a . Since z_V is only the counterexample with the largest violation, but not necessarily the whole region preventing certification, the half-space constraint obtained from a high κ might not be sufficient to separate this region from T . Thus, in a subsequent iteration, another half-space constraint for the same region may be added. For low κ , fewer constraints are required, but more verifiable volume of T is lost. Based on these considerations we outline our choices of κ in App. D.3.

7 Experimental Evaluation

We now extensively evaluate our hypotheses posed in §2 in §7.1 as well as experimentally evaluate the proposed proof

transfer method. In §7.2 and §7.3 we discuss robustness verification for adversarial patches (§5.2) and geometric perturbations (§5.3), respectively. Then, in §7.4 we investigate ℓ_∞ -robustness as discussed in §6.2.

All experiments are implemented in PyTorch [34], using the Gurobi Solver [19] for exact verification and evaluated on an Intel Core i9-9900K CPU. For all timing results we provide the mean over three runs.

Table 1. Overlap and containment of box verification for 5x100 on pairs of semantically similar inputs, pairs of random inputs from the same class, and randomly sampled inputs.

Layer l	o_p^l					$c_{0.9}^l$	
	1	2	3	4	5	4	5
$\epsilon = 0.1, p = 0.9$							
Similar	0.06	0.05	0.21	0.70	0.88	0.02	0.06
Class rand.	0.00	0.00	0.01	0.09	0.14	0.00	0.01
Random	0.00	0.00	0.00	0.00	0.01	0.00	0.00
$\epsilon = 0.2, p = 0.99$							
Similar	0.04	0.09	0.36	0.80	0.92	0.03	0.08
Class rand.	0.00	0.00	0.00	0.02	0.06	0.00	0.01
Random	0.00	0.00	0.01	0.02	0.03	0.00	0.00

7.1 Hypotheses for Robustness Proofs

We now empirically investigate the hypotheses in §2.

Similar inputs produce similar abstract shapes. First we show Hypothesis 1, that is, semantically similar inputs regions produce abstract shapes which overlap significantly.

Here we consider \mathcal{I}_ϵ verification using the Box abstraction on robustly trained [31] neural networks for handwritten digit [26] classification. We consider two neural networks, a feed forward neural network, 5x100, as well as a convolutional neural network (CNN) (details in App. D.1). Further, we consider semantic similarity as closeness (in Euclidean distance) at intermediate layers (same metric as Krizhevsky et al. [24]). For a pair of two abstract shapes at a layer l with d dimensions, we consider two measurement indicators:

- o_p^l , which indicates whether the activations in at least $p \cdot d$ dimensions overlap (for $p \in [0, 1]$).
- c_p^l , which indicates whether one abstract shape contains at least $p \cdot d$ dimensions of the other (for $p \in [0, 1]$). Note that for $p = 1.0$ this denotes full containment of one shape in the other.

In Table 1 we provide the average of these metrics for pairs of semantically similar inputs, random pairs from the same class and completely random pairs. For the random inputs we sample 200 verifiable inputs from the test set and then consider all $\binom{200}{2}$ possible pairs. For the class conditional random inputs we do the same but only sample from one class. In order to obtain the similar inputs, we first pick 1000

Table 2. Average size of X_x , whether the union could be verified and how many half-space constraints (on average) were required to do so.

Net	ϵ	$ X_V $	verif.	#H
5x100	0.1	5.77	0.97	0.01
5x100	0.2	5.56	0.96	0.00
CNN	0.1	5.82	0.94	0.40
CNN	0.2	5.68	0.94	0.18

verifiable inputs x . For each, we then find their 5 closest semantic neighbors via the ℓ_2 distance of their concrete activations in an intermediate layer k (we use $k = 4$ for 5x100 and $k = 5$ for the CNN) and then discard those that are not verifiable. This results in a set X_x of up to 6 verifiable inputs. We then consider all possible pairs of two in this set. The results in Table 1 consider the abstraction pre-ReLU in each layer. The activations after the ReLU show the same trend, but inflate the overlap numbers due to many dimensions being set to zero. We observe significant overlap for similar inputs and much lower overlap for randomly selected pairs. This result verifies what is to be expected from prior results on concrete activations [24, 45]. Results for the CNN, on which we observe similar results, are provided in App. D.1.

Convex hulls of abstract shapes are verifiable. Next, to investigate Hypothesis 2, we show that convex hulls of intermediate abstract shapes for similar input regions are verifiable. To this end we consider the previously defined X_x and compute the join over these sets, as standard: $\sqcup_D(\{V(x, N_{1:k}) \mid x \in X_V\})$. We then attempt to verify these unions using the exact verifier V [46] and up to 30 half-space constraints as outlined in §6.3. We show results in Table 2. From the size (close to 6) we observe that on average most inputs are verifiable and that indeed most unions are verifiable. For these small regions, especially on 5x100, only few half-space constraints are needed.

This high percentage of verifiable unions is particularly surprising as in Table 1 we only rarely see containment c_p^l .

Some \mathcal{I} imply others. To substantiate Hypothesis 3, we consider 1000 x for which \mathcal{I}_ϵ can be verified using the Box abstraction. For each of these we then sample 2 random 2×2 patch locations and check whether the propagation of $\mathcal{I}_{2 \times 2}^{i,j}(x)$ is included in the abstract shape of $\mathcal{I}_\epsilon(x)$ at layer k . For the 5x100 with $\epsilon = 0.1$ and 0.2 we observe that 73 and 77 % of the abstract shapes obtained for patch perturbations were contained in the abstract shape of the ℓ_∞ perturbation. For the CNN with $\epsilon = 0.1, 0.2$ and 0.3, we observe 10, 14 and 20 %, respectively. As is to be expected, larger input regions lead to more containment.

Table 3. 2×2 patch verification for different combinations of template layers k , 7x200 networks, using $m = 1$ template.

	shapes matched to template at layer							verif. acc.		
	k	1	2	3	4	5	6	7		
MNIST	0.186	0.856	0.941	0.952	0.955	0.957	0.957	0.970		
CIFAR	0.001	0.271	0.337	0.344	0.342	0.342	0.343	0.422		
verification time										
	k	-	1	2	3	4	1+3	2+3	2+4	2+3+4
MNIST	2.10	1.94	1.15	1.22	1.41	1.27	1.09	1.10	1.14	
CIFAR	3.27	2.98	2.53	2.32	2.47	2.35	2.49	2.42	2.55	

7.2 Robustness against adversarial patches

Now we show the application of proof transfer to the verification of robustness to adversarial patch attacks §5.2. Here, we again investigate the MNIST dataset [26], along with the CIFAR dataset [23] on 100 images each. As the baseline V_Q and V_T , we use Zonotope propagation. For both datasets we consider 7x200 and 9x500 robustly trained feed forward networks. We provide further details in App. D.4.

For the MNIST dataset containing 28×28 images, as outlined in §5.2, in order to verify inputs to be robust against 2×2 patch perturbations, 729 individual perturbations must be verified. Only if all of these are verified, the overall property can be verified for this input. Similarly, for CIFAR, containing 32×32 color images, there are 961 perturbations to be verified. Note that the patch is applied over all color channels.

The algorithm discussed in §5.2 has two main parameters: the considered pixel locations π_1, \dots, π_m and the layers at which templates are generated. We now investigate both.

We first study the impact of the used layer. To this end we consider the 7x200 networks, use $m = 1$ with π_1 that covers the whole image (equivalent to \mathcal{I}_ϵ for the maximal verifiable ϵ). Table 3 shows the corresponding template matching rates and verification times (including the template generation) respectively. From this we conclude that many template matches can already be made at the second or third layer. We find that in terms of verification time, creating templates simultaneously at the second and third layer, using the method outlined in §5.2, works best overall. For further experiments in the section we thus use these two layers.

Next, we investigate the impact of the pixel masks π_1, \dots, π_m . To this end we consider three different settings: (i) the full image (ℓ_∞ -mask as before), (ii) "center + border" ($m = 1$), where we consider the 6×6 center and all other pixels ($m = 2$), and (iii) the 2×2 grid ($m = 4$) where we split the image into equally sized quarters. As before, during template generation, we maximize the value of ϵ for each π_i .

As we can see in Table 4, the more templates are used, the more abstract shapes can be matched to the templates,

Table 4. 2×2 patch verification with templates at the 2nd & 3rd layer of the 7x200 networks for different masks.

Method/Mask	num templates	patch matches	run time
Baseline	-	-	2.14
L-infinity	1	0.941	1.11
Center + Border	2	0.946	1.41
2×2 Grid	4	0.950	3.49

Table 5. 2×2 patch verification with templates generated on the second and third layer using the ℓ_∞ -mask. Verification times are given for the baseline t^{BL} and for applying proof transfer t^{PT} in seconds per image.

Dataset	Net	verif. acc.	t^{BL}	t^{PT}	patch mat.	patch verif.
MNIST	7x200	0.81	2.10	1.10	0.941	0.970
	9x500	0.96	2.70	1.32	0.930	0.953
CIFAR	7x200	0.29	3.28	2.45	0.337	0.422
	9x500	0.28	5.48	4.48	0.342	0.609

Table 6. $\pm 2^\circ$ rotation, $\pm 10\%$ contrast and $\pm 1\%$ brightness change split into n_S perturbations on 100 MNIST images. (left) Verification rate & run time of zonotope t^{BL} and proof transfer t^{PT} . (right) Rate of splits matched and rate of splits verified to template.

n_S	verif.	t^{BL}	t^{PT}	n_S	splits matched	splits verif.
4	0.73	3.06	1.87	4	0.731	0.873
6	0.91	9.29	3.81	6	0.910	0.948
8	0.93	20.64	7.48	8	0.942	0.959
10	0.95	38.50	13.38	10	0.949	0.965

indicating that our optimization procedure is a good approximation to Problem 2. However, as $m > 1$ methods are only marginally better than the ℓ_∞ -mask, verification time gained by these additional matches does not offset the time spent to create additional templates. This shows that simple templates result in a better trade-off.

Based on this investigation we now, in Table 5, evaluate all networks and datasets using $m = 1$ and template generation at layers 2 and 3. In all cases, we obtain a speed up between 18% to 51% over the baseline verification.

7.3 Robustness against geometric perturbations

For the verification of geometric perturbations we take 100 images from the MNIST dataset and the 7x200 neural network from §7.2. Again, as the baseline V_Q and V_T , we use Zonotope propagation. As in §7.2 we create templates at the second and third layers.

In Table 6, we consider an input specification with $\pm 2^\circ$ rotation followed by a $\pm 10\%$ contrast and $\pm 1\%$ brightness change.

Table 7. $\pm 40^\circ$ rotation split into 200 perturbations evaluated on 100 MNIST. The verification rate is 0.15, but 0.821 of individual splits can be verified.

Method	m	splits matched	verif. time
Baseline	-	-	11.79
Proof Transfer	1	0.380	9.15
	2	0.411	9.21
	3	0.585	8.34

Table 8. Template matching rate and verification time of the whole MNIST test set t in seconds for the 5x100 using up to m templates per label and layer pair. The baseline verification 292.13 and 291.80 seconds for $\epsilon = 0.05$ and $\epsilon = 0.10$ respectively. We use Box templates with template expansion.

B+	k	shapes matched			verification time [s]		
		$m = 1$	$m = 3$	$m = 25$	$m = 1$	$m = 3$	$m = 25$
$\epsilon = 0.05$							
	3	0.078	0.150	0.305	284.27	274.26	257.77
	4	0.201	0.389	0.590	280.44	268.97	258.02
	3+4	0.213	0.360	0.606	275.31	260.95	241.36
$\epsilon = 0.10$							
	3	0.054	0.106	0.212	285.76	278.94	266.85
	4	0.156	0.305	0.477	285.15	274.82	266.62
	3+4	0.163	0.315	0.492	280.49	269.90	257.82

To certify the input region we consider its overapproximation in the Box domain as considered in Balunovic et al. [4], and split it n_S times. Here we use $m = 1$, a single template, optimized for maximal ϵ . We observe that as we increase n_S , verification rate increases, but also the speed ups obtained from proof transfer.

Next we investigate the impact of the number of templates m . For this we consider a $\pm 40^\circ$ rotation generated input region with $n_S = 200$. In Table 7 we evaluate this for m templates obtained from the maximal ℓ_∞ input perturbation around m equally spaced rotations. Again we observe that while $m > 1$ allows more templates matches, but in this case $m = 3$ is faster than $m = 1$.

7.4 ℓ_∞ certification with dataset templates

Here we instantiate the algorithm presented in §6.2 for the MNIST dataset. We first consider templates expressed in the Box domain, and investigate Stars with additional half-space later. We generate the set of templates \mathcal{T} individually for each label. Here, we consider the 5x100 network as in §7.1 and apply template generation individually per label at the third and fourth layers. We allow up to $m = 25$ templates and use template expansion (App. B). For $\epsilon = 0.05$ we found between 6 and 24 templates per label and layer.

In Table 8 we provide the fraction of input regions that could be successfully matched to templates as well as the overall verification time. We see that the templates can subsume up to 60.6% of input regions in the test set with $\epsilon = 0.05$, and up to 49.2% for higher $\epsilon = 0.1$. If an input cannot be matched with any of the templates, then we propagate the standard Zonotope abstract shape through the rest of the network to verify it. Combining template at multiple layers gives more matched templates as many inputs can be matched in the third layer, while unmatched ones can again be considered at the fourth layer. We observe that improvements in matching rate directly lead to speed ups over standard verification.

Additionally allowing half-space constraints, that is use Stars instead of Boxes as templates, allows us to increase the matching rate up to 65.2 % and 54.5 % for the two ϵ respectively. However, as checking matches for Stars is computationally more expensive the verification time does not improve further. For a full comparison see Table 12 in App. E.2.

For the CNN (same as in §7.1; results provided in App. E.2). We observe higher matching rates compared to the 5x100 network. There however the difference in verification time in comparison to the standard verification is negligible. The reason for this is that we found templates to only work well in the linear layers, which are late in the architecture, thus diminishing run time gains.

These results highlight, that with the algorithm outlined in §6.2, a set of templates \mathcal{T} can be obtained that generalize remarkably well to new input regions (e.g., up to 65.2 % containment). That is, while more precise domains such as stars allow templates that capture a far higher rate of containment for new input regions, their added cost of the containment check makes the obtained speedups smaller.

8 Conclusion

In this work we have, for the first time, studied the similarities of proofs for neural network verification, and formulated several key hypotheses about robustness proofs.

Then based on these hypotheses, we introduced the novel concept of proof transfer, which we instantiated in both online and offline settings. We achieve up to 2x speedup in the online setting and generalization of 65% to unseen inputs in the offline setting. We believe that the ideas described in this work can serve as a solid foundation for exploring methods that effectively share proofs in neural network verification.

References

[1] Ross Anderson, Joey Huchette, Christian Tjandraatmadja, and Juan Pablo Vielma. 2019. Strong Mixed-Integer Programming Formulations for Trained Neural Networks. In *Proc. Integer Programming and Combinatorial Optimization (IPCO) (Lecture Notes in Computer Science, Vol. 11480)*. 27–42.

[2] Pranav Ashok, Vahid Hashemi, Jan Kretínský, and Stefanie Mohr. 2020. DeepAbstract: Neural Network Abstraction for Accelerating Verification. In *Automated Technology for Verification and Analysis - 18th International Symposium, ATVA 2020, Hanoi, Vietnam, October 19-23, 2020, Proceedings (Lecture Notes in Computer Science, Vol. 12302)*, Dang Van Hung and Oleg Sokolsky (Eds.). Springer, 92–107. https://doi.org/10.1007/978-3-030-59152-6_5

[3] Stanley Bak and Parasara Sridhar Duggirala. 2017. Simulation-equivalent reachability of large linear systems with inputs. In *International Conference on Computer Aided Verification*. Springer, 401–420.

[4] Mislav Balunovic, Maximilian Baader, Gagandeep Singh, Timon Gehr, and Martin T. Vechev. 2019. Certifying Geometric Robustness of Neural Networks. In *NeurIPS*. 15287–15297.

[5] Mislav Balunovic and Martin Vechev. 2020. Adversarial Training and Provable Defenses: Bridging the Gap. In *International Conference on Learning Representations*. <https://openreview.net/forum?id=SJxSDxrKDr>

[6] Battista Biggio, Igino Corona, Davide Maiorca, Blaine Nelson, Nedim Srndic, Pavel Laskov, Giorgio Giacinto, and Fabio Roli. 2013. Evasion Attacks against Machine Learning at Test Time. In *ECML/PKDD (3) (Lecture Notes in Computer Science, Vol. 8190)*. Springer, 387–402.

[7] Elena Botoeva, Panagiotis Kouvaros, Jan Kronqvist, Alessio Lomuscio, and Ruth Misener. 2020. Efficient Verification of ReLU-Based Neural Networks via Dependency Analysis. In *Proc. AAAI Conference on Artificial Intelligence (AAAI)*. 3291–3299.

[8] Rudy Bunel, Jingyue Lu, Ilker Turkaslan, Philip H. S. Torr, Pushmeet Kohli, and M. Pawan Kumar. 2020. Branch and Bound for Piecewise Linear Neural Network Verification. *J. Mach. Learn. Res.* 21 (2020), 42:1–42:39.

[9] Rudy Bunel, Ilker Turkaslan, Philip H. S. Torr, Pushmeet Kohli, and Pawan Kumar Mudigonda. 2018. A Unified View of Piecewise Linear Neural Network Verification. In *Advances in Neural Information Processing Systems 31: Annual Conference on Neural Information Processing Systems 2018, NeurIPS 2018, 3-8 December 2018, Montréal, Canada.*, Samy Bengio, Hanna M. Wallach, Hugo Larochelle, Kristen Grauman, Nicolò Cesa-Bianchi, and Roman Garnett (Eds.). 4795–4804. <http://papers.nips.cc/paper/7728-a-unified-view-of-piecewise-linear-neural-network-verification>

[10] Chih-Hong Cheng and Rongjie Yan. 2020. Continuous Safety Verification of Neural Networks. *CoRR* abs/2010.05689 (2020). arXiv:2010.05689 <https://arxiv.org/abs/2010.05689>

[11] Ping-Yeh Chiang, Renkun Ni, Ahmed Abdelkader, Chen Zhu, Christoph Studer, and Tom Goldstein. 2020. Certified Defenses for Adversarial Patches. In *8th International Conference on Learning Representations, ICLR 2020, Addis Ababa, Ethiopia, April 26-30, 2020*. OpenReview.net. <https://openreview.net/forum?id=HyeaSkrYPH>

[12] Krishnamurthy Dvijotham, Robert Stanforth, Sven Gowal, Timothy Mann, and Pushmeet Kohli. 2018. A Dual Approach to Scalable Verification of Deep Networks. In *Proc. Uncertainty in Artificial Intelligence (UAI)*. 162–171.

[13] Krishnamurthy (Dj) Dvijotham, Robert Stanforth, Sven Gowal, Chongli Qin, Soham De, and Pushmeet Kohli. 2019. Efficient Neural Network Verification with Exactness Characterization. In *Proc. Uncertainty in Artificial Intelligence, UAI*. 164.

[14] Rüdiger Ehlers. 2017. Formal Verification of Piece-Wise Linear Feed-Forward Neural Networks. In *Automated Technology for Verification and Analysis - 15th International Symposium, ATVA 2017, Pune, India, October 3-6, 2017, Proceedings (Lecture Notes in Computer Science, Vol. 10482)*, Deepak D’Souza and K. Narayan Kumar (Eds.). Springer, 269–286. https://doi.org/10.1007/978-3-319-68167-2_19

[15] Logan Engstrom, Andrew Ilyas, Shibani Santurkar, Dimitris Tsipras, Brandon Tran, and Aleksander Madry. 2019. Learning Perceptually-Aligned Representations via Adversarial Robustness. *CoRR* abs/1906.00945 (2019). arXiv:1906.00945 <http://arxiv.org/abs/1906.00945>

[16] Marc Fischer, Maximilian Baader, and Martin Vechev. 2020. Certified Defense to Image Transformations via Randomized Smoothing. In *Advances in Neural Information Processing Systems 33*.

[17] Timon Gehr, Matthew Mirman, Dana Drachsler-Cohen, Petar Tsankov, Swarat Chaudhuri, and Martin T. Vechev. 2018. AI2: Safety and Robustness Certification of Neural Networks with Abstract Interpretation. In *2018 IEEE Symposium on Security and Privacy, SP 2018, Proceedings, 21-23 May 2018, San Francisco, California, USA*. IEEE Computer Society, 3–18. <https://doi.org/10.1109/SP.2018.00058>

[18] Sven Gowal, Krishnamurthy Dvijotham, Robert Stanforth, Rudy Bunel, Chongli Qin, Jonathan Uesato, Relja Arandjelovic, Timothy A. Mann, and Pushmeet Kohli. 2018. On the Effectiveness of Interval Bound Propagation for Training Verifiably Robust Models. *CoRR* abs/1810.12715 (2018). arXiv:1810.12715 <http://arxiv.org/abs/1810.12715>

[19] LLC Gurobi Optimization. 2020. Gurobi Optimizer Reference Manual. <http://www.gurobi.com>

[20] Andrew Ilyas, Shibani Santurkar, Dimitris Tsipras, Logan Engstrom, Brandon Tran, and Aleksander Madry. 2019. Adversarial Examples Are Not Bugs, They Are Features. In *Advances in Neural Information Processing Systems 32: Annual Conference on Neural Information Processing Systems 2019, NeurIPS 2019, 8-14 December 2019, Vancouver, BC, Canada*, Hanna M. Wallach, Hugo Larochelle, Alina Beygelzimer, Florence d’Alché-Buc, Emily B. Fox, and Roman Garnett (Eds.). 125–136. <http://papers.nips.cc/paper/8307-adversarial-examples-are-not-bugs-they-are-features>

[21] Guy Katz, Clark W. Barrett, David L. Dill, Kyle Julian, and Mykel J. Kochenderfer. 2017. Reluplex: An Efficient SMT Solver for Verifying Deep Neural Networks. In *Computer Aided Verification - 29th International Conference, CAV 2017, Heidelberg, Germany, July 24-28, 2017, Proceedings, Part I (Lecture Notes in Computer Science, Vol. 10426)*, Rupak Majumdar and Viktor Kuncak (Eds.). Springer, 97–117. https://doi.org/10.1007/978-3-319-63387-9_5

[22] Guy Katz, Derek A. Huang, Duligur Ibeling, Kyle Julian, Christopher Lazarus, Rachel Lim, Parth Shah, Shantanu Thakoor, Haoze Wu, Aleksandar Zelić, David L. Dill, Mykel J. Kochenderfer, and Clark Barrett. 2019. The Marabou Framework for Verification and Analysis of Deep Neural Networks. In *Proc. Computer Aided Verification (CAV)*. 443–452.

[23] Alex Krizhevsky, Geoffrey Hinton, et al. 2009. Learning multiple layers of features from tiny images. (2009).

[24] Alex Krizhevsky, Ilya Sutskever, and Geoffrey E. Hinton. 2017. ImageNet classification with deep convolutional neural networks. *Commun. ACM* 60, 6 (2017), 84–90. <https://doi.org/10.1145/3065386>

[25] Alexey Kurakin, Ian J. Goodfellow, and Samy Bengio. 2017. Adversarial Machine Learning at Scale. In *5th International Conference on Learning Representations, ICLR 2017, Toulon, France, April 24-26, 2017, Conference Track Proceedings*. OpenReview.net. <https://openreview.net/forum?id=BJm4T4Kgx>

[26] Yann LeCun, Bernhard E. Boser, John S. Denker, Donnie Henderson, Richard E. Howard, Wayne E. Hubbard, and Lawrence D. Jackel. 1989. Handwritten Digit Recognition with a Back-Propagation Network. In *Advances in Neural Information Processing Systems 2, [NIPS Conference, Denver, Colorado, USA, November 27-30, 1989]*, David S. Touretzky (Ed.). Morgan Kaufmann, 396–404. <http://papers.nips.cc/paper/293-handwritten-digit-recognition-with-a-back-propagation-network>

[27] Linyi Li, Maurice Weber, Xiaojun Xu, Luka Rimanic, Tao Xie, Ce Zhang, and Bo Li. 2020. Provably Robust Learning Based on Transformation-Specific Smoothing. *CoRR* abs/2002.12398 (2020).

[28] Jingyue Lu and M. Pawan Kumar. 2020. Neural Network Branching for Neural Network Verification. In *Proc. International Conference on Learning Representations (ICLR)*.

[29] Laurens van der Maaten and Geoffrey Hinton. 2008. Visualizing data using t-SNE. *Journal of machine learning research* 9, Nov (2008), 2579–2605.

[30] Aleksander Madry, Aleksandar Makelov, Ludwig Schmidt, Dimitris Tsipras, and Adrian Vladu. 2018. Towards Deep Learning Models Resistant to Adversarial Attacks. In *6th International Conference on Learning Representations, ICLR 2018, Vancouver, BC, Canada, April 30 - May 3, 2018, Conference Track Proceedings*. OpenReview.net. <https://openreview.net/forum?id=rJzIBfZAb>

[31] Matthew Mirman, Timon Gehr, and Martin T. Vechev. 2018. Differentiable Abstract Interpretation for Provably Robust Neural Networks. In *Proceedings of the 35th International Conference on Machine Learning, ICML 2018, Stockholmsmässan, Stockholm, Sweden, July 10-15, 2018 (Proceedings of Machine Learning Research, Vol. 80)*, Jennifer G. Dy and Andreas Krause (Eds.). PMLR, 3575–3583. <http://proceedings.mlr.press/v80/mirman18b.html>

[32] Jeet Mohapatra, Tsui-Wei Weng, Pin-Yu Chen, Sijia Liu, and Luca Daniel. 2019. Towards Verifying Robustness of Neural Networks Against Semantic Perturbations. *CoRR* abs/1912.09533 (2019).

[33] Jeet Mohapatra, Tsui-Wei Weng, Pin-Yu Chen, Sijia Liu, and Luca Daniel. 2020. Towards Verifying Robustness of Neural Networks Against A Family of Semantic Perturbations. In *2020 IEEE/CVF Conference on Computer Vision and Pattern Recognition, CVPR 2020, Seattle, WA, USA, June 13-19, 2020*. IEEE, 241–249. <https://doi.org/10.1109/CVPR42600.2020.00032>

[34] Adam Paszke, Sam Gross, Francisco Massa, Adam Lerer, James Bradbury, Gregory Chanan, Trevor Killeen, Zeming Lin, Natalia Gimelshein, Luca Antiga, Alban Desmaison, Andreas Kopf, Edward Yang, Zachary DeVito, Martin Raison, Alykhan Tejani, Sasank Chilamkurthy, Benoit Steiner, Lu Fang, Junjie Bai, and Soumith Chintala. 2019. PyTorch: An Imperative Style, High-Performance Deep Learning Library. In *Advances in Neural Information Processing Systems 32*, H. Wallach, H. Larochelle, A. Beygelzimer, F. d’Alché-Buc, E. Fox, and R. Garnett (Eds.). Curran Associates, Inc., 8024–8035. <http://papers.neurips.cc/paper/9015-pytorch-an-imperative-style-high-performance-deep-learning-library.pdf>

[35] Brandon Paulsen, Jingbo Wang, and Chao Wang. 2020. ReluDiff: differential verification of deep neural networks. In *ICSE '20: 42nd International Conference on Software Engineering, Seoul, South Korea, 27 June - 19 July, 2020*, Gregg Rothermel and Doo-Hwan Bae (Eds.). ACM, 714–726. <https://doi.org/10.1145/3377811.3380337>

[36] Brandon Paulsen, Jingbo Wang, Jiawei Wang, and Chao Wang. 2020. NeuroDiff: Scalable Differential Verification of Neural Networks using Fine-Grained Approximation. *CoRR* abs/2009.09943 (2020). arXiv:2009.09943 <https://arxiv.org/abs/2009.09943>

[37] Kexin Pei, Yinzhi Cao, Junfeng Yang, and Suman Jana. 2017. Towards Practical Verification of Machine Learning: The Case of Computer Vision Systems. *CoRR* abs/1712.01785 (2017). arXiv:1712.01785 <http://arxiv.org/abs/1712.01785>

[38] Aditi Raghunathan, Jacob Steinhardt, and Percy Liang. 2018. Semidefinite relaxations for certifying robustness to adversarial examples. In *Advances in Neural Information Processing Systems 31: Annual Conference on Neural Information Processing Systems 2018, NeurIPS 2018, 3-8 December 2018, Montréal, Canada*, Samy Bengio, Hanna M. Wallach, Hugo Larochelle, Kristen Grauman, Nicolò Cesa-Bianchi, and Roman Garnett (Eds.). 10900–10910. <http://papers.neurips.cc/paper/8285-semidefinite-relaxations-for-certifying-robustness-to-adversarial-examples>

[39] Volker Roth, Julian Laub, Motoaki Kawanabe, and Joachim M. Buhmann. 2003. Optimal Cluster Preserving Embedding of Nonmetric Proximity Data. *IEEE Trans. Pattern Anal. Mach. Intell.* 25, 12 (2003), 1540–1551. <https://doi.org/10.1109/TPAMI.2003.1251147>

[40] Wenjie Ruan, Xiaowei Huang, and Marta Kwiatkowska. 2018. Reachability Analysis of Deep Neural Networks with Provable Guarantees. In *Proc. International Joint Conference on Artificial Intelligence, (IJCAI)*.

[41] Hadi Salman, Greg Yang, Huan Zhang, Cho-Jui Hsieh, and Pengchuan Zhang. 2019. A Convex Relaxation Barrier to Tight Robustness Verification of Neural Networks. In *NeurIPS*. 9832–9842.

[42] David Silver, Julian Schrittwieser, Karen Simonyan, Ioannis Antonoglou, Aja Huang, Arthur Guez, Thomas Hubert, Lucas Baker, Matthew Lai, Adrian Bolton, et al. 2017. Mastering the game of go without human knowledge. *Nature* 550, 7676 (2017), 354.

[43] Gagandeep Singh, Timon Gehr, Matthew Mirman, Markus Püschel, and Martin T. Vechev. 2018. Fast and Effective Robustness Certification. In *Advances in Neural Information Processing Systems 31: Annual Conference on Neural Information Processing Systems 2018, NeurIPS 2018, 3-8 December 2018, Montréal, Canada*, Samy Bengio, Hanna M. Wallach, Hugo Larochelle, Kristen Grauman, Nicolò Cesa-Bianchi, and Roman Garnett (Eds.). 10825–10836. <http://papers.nips.cc/paper/8278-fast-and-effective-robustness-certification>

[44] Gagandeep Singh, Timon Gehr, Markus Püschel, and Martin T. Vechev. 2019. An abstract domain for certifying neural networks. *PACMPL* 3, POPL (2019), 41:1–41:30. <https://doi.org/10.1145/3290354>

[45] Christian Szegedy, Wojciech Zaremba, Ilya Sutskever, Joan Bruna, Dumitru Erhan, Ian J. Goodfellow, and Rob Fergus. 2014. Intriguing properties of neural networks. In *2nd International Conference on Learning Representations, ICLR 2014, Banff, AB, Canada, April 14-16, 2014, Conference Track Proceedings*, Yoshua Bengio and Yann LeCun (Eds.). <http://arxiv.org/abs/1312.6199>

[46] Vincent Tjeng, Kai Y. Xiao, and Russ Tedrake. 2019. Evaluating Robustness of Neural Networks with Mixed Integer Programming. In *ICLR (Poster)*. OpenReview.net.

[47] Hoang-Dung Tran, Xiaodong Yang, Diego Manzanas Lopez, Patrick Musau, Luan Viet Nguyen, Weiming Xiang, Stanley Bak, and Taylor T. Johnson. 2020. NNV: The Neural Network Verification Tool for Deep Neural Networks and Learning-Enabled Cyber-Physical Systems. *CoRR* abs/2004.05519 (2020).

[48] Hoang-Dung Tran, Diago Manzanas Lopez, Patrick Musau, Xiaodong Yang, Luan Viet Nguyen, Weiming Xiang, and Taylor T. Johnson. 2019. Star-based reachability analysis of deep neural networks. In *International Symposium on Formal Methods*. Springer, 670–686.

[49] Dimitris Tsipras, Shibani Santurkar, Logan Engstrom, Alexander Turner, and Aleksander Madry. 2019. Robustness May Be at Odds with Accuracy. In *7th International Conference on Learning Representations, ICLR 2019, New Orleans, LA, USA, May 6-9, 2019*. OpenReview.net. <https://openreview.net/forum?id=SyxAh30cY7>

[50] Shiqi Wang, Kexin Pei, Justin Whitehouse, Junfeng Yang, and Suman Jana. 2018. Efficient Formal Safety Analysis of Neural Networks. In *Proc. Advances in Neural Information Processing Systems (NeurIPS)*. 6369–6379.

[51] Tsui-Wei Weng, Huan Zhang, Hongge Chen, Zhao Song, Cho-Jui Hsieh, Luca Daniel, Duane S. Boning, and Inderjit S. Dhillon. 2018. Towards Fast Computation of Certified Robustness for ReLU Networks. In *Proceedings of the 35th International Conference on Machine Learning, ICML 2018, Stockholmsmässan, Stockholm, Sweden, July 10-15, 2018 (Proceedings of Machine Learning Research, Vol. 80)*, Jennifer G. Dy and Andreas Krause (Eds.). PMLR, 5273–5282. <http://proceedings.mlr.press/v80/weng18a.html>

[52] Eric Wong and J. Zico Kolter. 2018. Provable Defenses against Adversarial Examples via the Convex Outer Adversarial Polytope. In *Proceedings of the 35th International Conference on Machine Learning, ICML 2018, Stockholmsmässan, Stockholm, Sweden, July 10-15, 2018 (Proceedings of Machine Learning Research, Vol. 80)*, Jennifer G. Dy and Andreas Krause (Eds.). PMLR, 5283–5292. <http://proceedings.mlr.press/v80/wong18a.html>

- [53] Huan Zhang, Hongge Chen, Chaowei Xiao, Sven Gowal, Robert Stanforth, Bo Li, Duane S. Boning, and Cho-Jui Hsieh. 2020. Towards Stable and Efficient Training of Verifiably Robust Neural Networks. In *8th International Conference on Learning Representations, ICLR 2020, Addis Ababa, Ethiopia, April 26-30, 2020*. OpenReview.net. <https://openreview.net/forum?id=Skxuk1rFwB>
- [54] Huan Zhang, Tsui-Wei Weng, Pin-Yu Chen, Cho-Jui Hsieh, and Luca Daniel. 2018. Efficient Neural Network Robustness Certification with General Activation Functions. In *Advances in Neural Information Processing Systems 31: Annual Conference on Neural Information Processing Systems 2018, NeurIPS 2018, 3-8 December 2018, Montréal, Canada*, Samy Bengio, Hanna M. Wallach, Hugo Larochelle, Kristen Grauman, Nicolò Cesa-Bianchi, and Roman Garnett (Eds.). 4944–4953. <http://papers.nips.cc/paper/7742-efficient-neural-network-robustness-certification-with-general-activation-functions>
- [55] Hongyang Zhang, Yaodong Yu, Jiantao Jiao, Eric P. Xing, Laurent El Ghaoui, and Michael I. Jordan. 2019. Theoretically Principled Trade-off between Robustness and Accuracy. In *Proceedings of the 36th International Conference on Machine Learning, ICML 2019, 9-15 June 2019, Long Beach, California, USA (Proceedings of Machine Learning Research, Vol. 97)*, Kamalika Chaudhuri and Ruslan Salakhutdinov (Eds.). PMLR, 7472–7482. <http://proceedings.mlr.press/v97/zhang19p.html>

A Impact of Adversarial Examples on Proof Similarity

In the discussion in §2, adversarial examples [6, 45], slightly perturbed inputs, that yield vastly different activations and classification appear to violate the similarity property stated by Krizhevsky et al. [24]. As was found by Szegedy et al. [45] this is indeed the case.

However in §2 we consider neural networks, trained to be robust to such perturbations [5, 18, 25, 30, 31, 53, 55], on which the similarity property is further *strengthened*, as they not just eliminate adversarial examples from violating it, but also better align their features with natural human semantics [15, 20, 49].

B Template Expansion

Algorithm 2: Template expansion

Input: $\mathcal{T} = \{T_i\}_{i=1}^m$, scaling matrix D , verifier V_T
Result: Set \mathcal{T}' of expanded templates, $|\mathcal{T}'| = m$

```

1 for  $i \leftarrow 1$  to  $k$  do
2    $T \leftarrow T_i$ 
3   while  $V_T(T, N_{k+1:L}) \vdash \psi$  do
4      $T_i \leftarrow T$ 
5     scale all dimensions of  $T$  according to  $D$ 
6   end
7 end
8 return  $\mathcal{T}' = \{T_i\}_{i=1}^m$ 
```

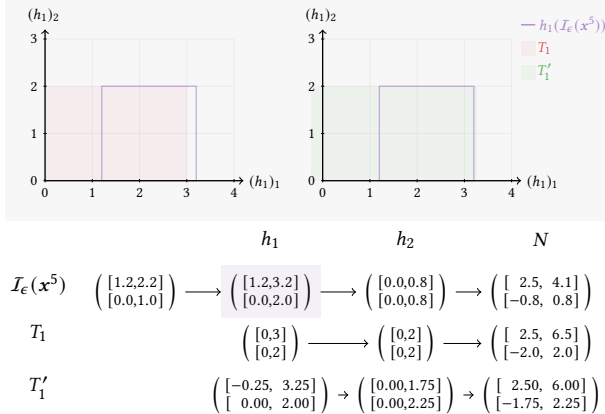


Figure 9. Continuation of the example given in §3 showcasing the template expansion algorithm. While the template T_1 does not subsume $h_1(I_\epsilon x^5)$ the expanded template T'_1 does.

Template Expansion. To further improve the generalization from training set to test set, we introduce an operation called *template expansion*, outlined in Algorithm 2. For the scaling operation we utilize a diagonal matrix $D := \text{diag}(f_1, \dots, f_d)$, where $f_i \geq 1$ is the scaling factor for the i -th

dimension, e.g. $D = 1.1I$ would scale all dimensions by a factor 1.1.

Example (cont.) We illustrate this by an extending the running example, introduced in §3, in Fig. 9. On the left in Fig. 9, template T_1 (shaded red) is obtained as in §3 and the abstract shape $h_1(I_\epsilon(x^5))$ for a new input x^5 , is shown in purple. $h_1(I_\epsilon(x^4))$ overlaps with template T_1 but is not contained inside it.

By applying template expansion with $D = \text{diag}(\frac{7}{6}, 1)$, we obtain the template T'_1 , shaded in green on the right of Fig. 9. T'_1 can be verified and now also contains $h_1(I_\epsilon(x^5))$, thus allowing to shortcut the verification of $I_\epsilon(x^5)$.

We note that in this case one loop iteration of Algorithm 2 was performed (as expanding T'_1 further would yield a non-verifiable shape).

Half-space Constraints. When we use the star domain with half-space constraints to encode templates, the expansion only modifies the underlying box, but not the half-space constraints, since these have already been selected to be close to the decision boundary. However, we attempt to add new constraints during the expansion process if the verification fails.

C Details for Figs. 2 and 3

We use the same networks and settings as in §7.1. In Fig. 2a we show the post-ReLU activations, with 512 dimensions, in the fifth hidden layer of CNN. The two dimensional embedding is obtained via TSNE embedding [29], initialized with a 150-dimensional principal component analysis (PCA).

In Fig. 2b projection to two dimensions was obtained by applying (PCA) to the activation vectors of the 6 displayed points. The obtained linear projection operator was then applied to the relaxations. The red outline (their box join) was verified using exact verification - no half-space constraints were added.

Fig. 3 uses the same setup as used here to show proof subsumption, and the same PCA as Fig. 2b.

D Experimental Details

D.1 Details for §7.1 (Hypotheses for Robustness Proofs)

We consider two neural networks, a feed forward neural network “5x100” (with 5 layers of 100 neurons each) and a convolutional neural network “CNN” (architecture described in App. D.2). The 5x100 network has an accuracy of 0.94 and a certified accuracy of 0.93 and 0.92 for $\epsilon = 0.1$ and $\epsilon = 0.2$ respectively. For the CNN these numbers are 0.93, 0.91 and 0.88.

D.2 Convolutional Neural Network Architecture

Table 9. Architecture of the ConvBig network. All convolution layers and all but the last linear layers apply the ReLU function. The parameters for the convolutions are the kernel size k , stride s and padding p . The architecture does not allow for templates at earlier layers (the convolutional layers are too wide to make template generation computationally feasible)

Layer	Shape
Input	1x28x28
Convolution ($k=3, s=1, p=1$)	32x28x28
Convolution ($k=4, s=2, p=1$)	32x14x14
Convolution ($k=3, s=1, p=1$)	64x14x14
Convolution ($k=4, s=2, p=1$)	64x7x7
Flatten	3136
Linear	512
Linear	512
Linear	10

D.3 Details for §7.4 (ℓ_∞ certification with dataset templates)

For a `cluster_proofs` we set an initial cluster size depending on the number of verifiable images per label, in order that the clusters contain on average 50 images. For the verification of a cluster’s union, we allow up to $n_{hs} = 30$ half-space constraints and set κ of 0.05. Taking a low value leads to a larger truncation, but reduces the number of half-space constraints, which speeds up the template generation as well as the containment check at inference. We take the same values also for verifying unions after merging two clusters. For expanding the templates, we use up to 10 iterations, in which we widen by 5% in each dimension and then allow up to 10 hyperplanes to verify the expanded template. To avoid truncating previously verified volume, we increase κ linearly by 0.02 for each expansion step, starting with an initial κ of 0.4

D.4 Details for §7.2 (Robustness against adversarial patches)

The neural networks was trained using robust training [30] for patch attacks, as outlined in [11]. The 7x200 and 9x500 networks were trained for 600 epochs to achieve accuracies on MNIST [26] of 0.983 and 0.953 respectively. These same values for the CIFAR [23] dataset a 0.488 and 0.481 respectively. Further numbers can be found in Table 5.

Table 10. Overlap and containment of box verification for the CNN on pairs of semantically similar inputs, pairs of random inputs form the same class, and randomly sampled inputs.

Layer l	o_p^l						$\frac{c_{0.9}^l}{6}$
	1	2	3	4	5	6	
$\epsilon = 0.1, p = 0.9$							
Similar	1.00	0.07	0.02	0.01	0.22	0.43	0.02
Class rand.	0.99	0.00	0.00	0.00	0.00	0.01	0.00
Random	0.94	0.00	0.00	0.00	0.00	0.01	0.00
$\epsilon = 0.2, p = 0.99$							
Similar	0.15	0.00	0.00	0.01	0.31	0.69	0.05
Class rand.	0.01	0.00	0.00	0.00	0.02	0.14	0.01
Random	0.00	0.00	0.00	0.00	0.00	0.02	0.00

E Additional Experimental results

E.1 Additional Results for §7.1 (Hypotheses for Robustness Proofs)

In Table 10 we provide the same results as for 5x100. Interestingly we see high overlap in the first layer of the CNN is very large, which happens as in the first convolution the error bounds for all inputs covered by the convolutional kernel are added, resulting in very large shapes. In subsequent convolutions layers as the activations diversify and the overlap drops before the expected pattern emerges.

E.2 Additional Results for §7.4 (ℓ_∞ certification with dataset templates)

Here we present extended evaluation on the template generation in the offline setting.

Table 12 shows an extended version of Table 8.

Table 11. for the CNN Table 9 after the first linear layer. We create templates in the box as well as in the star domain and compare their matching rates for the individual labels.

We observe strong correlation between accuracy, verified accuracy and the matching rates. Labels with higher accuracy also tend to have higher matching rates, with the difference in-between the labels being more significant for the latter. The verification times in the Table 11 are pretty similar across the different template generation methods, which is reasoned by the fact, that the template layer is rather late, meaning that a large amount of the time is spent to create the proof up to that layer, therby reducing the benefit of early stopping the creation.

Adding half-space constraints to boxes allows them to have larger bounds and still be verifiable, with the half-space constraints truncating counterexamples from the templates. These stars can better approximate the decision boundaries, therby increasing the number of matches on average from 0.352 to 0.651. Unfortunately, this gain cannot be converted

Table 11. Accuracy, certified accuracy for $\epsilon = 0.1$ and verification time and matching rates for different template generation algorithms on the CNN Table 9. Templates are created after the first linear layer. The methods B and S refer to the box and star domain respectively. The latter describes boxes with additional half-space constraints. The additional superscripts +/- stand for template generation with/without template expansion.

label	acc	verif. acc.	verification time per image [s]				matching rates				
			baseline	B ⁻	B ⁺	S ⁻	S ⁺	B ⁻	B ⁺	S ⁻	S ⁺
0	0.99	0.97	169.78	168.64	168.44	173.34	178.28	0.500	0.522	0.751	0.810
1	0.98	0.96	186.35	185.24	184.45	187.52	191.16	0.690	0.727	0.858	0.886
2	0.95	0.91	171.38	171.22	171.09	174.60	176.12	0.369	0.400	0.655	0.664
3	0.94	0.89	165.83	165.85	165.84	168.79	177.47	0.188	0.198	0.517	0.594
4	0.91	0.87	155.49	155.50	155.39	158.37	158.34	0.181	0.208	0.522	0.534
5	0.94	0.88	147.08	147.33	147.21	150.81	152.17	0.034	0.061	0.548	0.599
6	0.97	0.95	160.36	159.99	159.90	164.38	165.10	0.449	0.478	0.757	0.789
7	0.89	0.84	158.38	157.74	157.35	160.41	161.88	0.418	0.439	0.594	0.657
8	0.90	0.84	152.48	152.93	152.84	155.58	155.69	0.159	0.166	0.400	0.429
9	0.88	0.82	153.11	152.68	152.89	155.23	156.68	0.219	0.234	0.467	0.509

Table 12. Extended version of Table 8. Template matching rate and verification time of the whole MNIST test set t in seconds for the 5x100 using up to m templates per label and layer pair. The baseline verification 292.13 and 291.80 seconds for $\epsilon = 0.05$ and $\epsilon = 0.10$ respectively. +TE indicates the use of Template Expansion.

Box	shapes matched			verification time [s]			Box+TE	shapes matched			verification time [s]				
	k	$m = 1$	$m = 3$	$m = 25$	$m = 1$	$m = 3$	$m = 25$	k	$m = 1$	$m = 3$	$m = 25$	$m = 1$	$m = 3$	$m = 25$	
$\epsilon = 0.05$								$\epsilon = 0.05$							
	3	0.075	0.144	0.284	282.60	275.32	259.87		3	0.078	0.150	0.305	284.27	274.26	257.77
	4	0.195	0.380	0.576	279.87	270.08	258.06		4	0.201	0.389	0.590	280.44	268.97	258.02
	3+4	0.207	0.393	0.592	274.86	259.19	243.11		3+4	0.213	0.360	0.606	275.31	260.95	241.36
$\epsilon = 0.10$								$\epsilon = 0.10$							
	3	0.051	0.102	0.194	286.67	280.45	272.01		3	0.054	0.106	0.212	285.76	278.94	266.85
	4	0.150	0.296	0.458	283.06	275.39	268.05		4	0.156	0.305	0.477	285.15	274.82	266.62
	3+4	0.158	0.307	0.474	281.14	272.17	257.92		3+4	0.163	0.315	0.492	280.49	269.90	257.82
Star	shapes matched			verification time [s]			Star+TE	shapes matched			verification time [s]				
k	$m = 1$	$m = 3$	$m = 25$	$m = 1$	$m = 3$	$m = 25$	k	$m = 1$	$m = 3$	$m = 25$	$m = 1$	$m = 3$	$m = 25$		
$\epsilon = 0.05$								$\epsilon = 0.05$							
	3	0.108	0.252	0.404	281.33	269.24	254.41		3	0.111	0.258	0.418	282.99	271.34	254.62
	4	0.258	0.403	0.627	282.51	281.68	271.63		4	0.259	0.406	0.636	282.98	281.51	270.44
	3+4	0.279	0.451	0.643	277.89	266.55	246.39		3+4	0.283	0.456	0.652	278.00	269.08	247.43
$\epsilon = 0.10$								$\epsilon = 0.10$							
	3	0.079	0.182	0.290	284.31	277.96	267.72		3	0.081	0.187	0.303	285.82	280.71	267.55
	4	0.202	0.319	0.510	285.68	286.16	278.29		4	0.203	0.323	0.528	285.49	286.34	276.14
	3+4	0.217	0.358	0.529	283.43	278.00	262.96		3+4	0.220	0.362	0.545	284.39	278.90	262.60

to a speed-up, due to the larger cost of the containment check for stars and the late template layer.

In both the CNN and the 5x100 network Template Expansion (App. B) leads to a higher matching rate and speed-ups.